

## Energy efficiency of an electric drive including the thermal feedback from the cooling loop

Master's thesis in Electric Power Engineering

**WINNIE MWANGI**



MASTER'S THESIS 2018:NN

**ENERGY EFFICIENCY OF AN ELECTRIC  
DRIVE INCLUDING THE THERMAL  
FEEDBACK FROM THE COOLING LOOP**

WINNIE MWANGI



**CHALMERS**  
UNIVERSITY OF TECHNOLOGY

Department of Energy and Environment  
*Electric power Engineering*  
CHALMERS UNIVERSITY OF TECHNOLOGY  
Gothenburg, Sweden 2018

Energy efficiency of an electric drive including the thermal feedback from the cooling loop

WINNIE MWANGI

© WINNIE MWANGI, 2018.

Supervisor: Magnus Johansson , NEVS

Examiner: Torbjörn Thiringer, Department of Energy and Environment

Department of Energy and Environment

Division of Electrical Engineering

Chalmers University of Technology

SE-412 96 Gothenburg

Telephone +46 31 772 1000

Cover: Energy efficiency of an electric drive including the thermal feedback from the cooling loop

Gothenburg, Sweden 2018

Energy efficiency of an electric drive including the thermal feedback from the cooling loop

WINNIE MWANGI

Department of Energy and Environment

Chalmers University of Technology

## Abstract

This project was performed in the powertrain department of National Electric Vehicle of Sweden (NEVS). Electric drive contributes a big percentage to the amount of power consumed globally. An electric drive has many components but the main one that lead to power consumption is the electric machine. In this thesis an electric machine is in the propulsion loop. With an efficiently operating electric machine the entire electric drive would be improved.

A study is done on the propulsion loop and its components for an energy efficient way of operating. A propulsion loop consists of a radiator, power electronic converters, an electric machine, an accumulator tank, a pump, pipes and fans.

Using manufacturers' data sheets, the above mentioned components were modelled in GT-SUITE software tool. A lumped thermal model of the electric machine was made where all its parts were modelled as thermal masses and the water jacket as flow. Volume was extracted to show the flow of the coolant in the electric machine. GT-SUITE has modelling objects that can be edited to suit the need.

It was achieved that a fan can operate at a different signal and cool as much as needed but at a lower power consumption. The pump was also observed to be able to pump at a lower flow rate and still achieve the needed cooling thus reducing the power consumed. It was also observed that the size of the radiator could be reduced as well.

The power electronic converters were not modelled to details since they were missing manufacturers' data. However, in the future they could be modelled and improve the loop efficiency further.

The component models were based on real object in a concept battery electric vehicle car at NEVS.

Keywords: Thermal modelling, Heat transfer, Energy efficiency, Propulsion loop, Losses, Driving cycle, Steady state.



# Acknowledgements

With a heart full of gratitude, it is a pleasure for me to thank all that made this thesis to be fulfilled.

First i would like to thank my supervisor and professor at Chalmers Torbjörn Thiringer for your patience, the technical guidance, emotional support and for finding this thesis topic. Sincere thanks to Emma Grundrit (postdoctrante) for your help in understanding this topic further.

I would like to thank the entire powertrain department, James Hildebrand as PowerTrain manager at NEVS, Magnus Johansson my supervisor at NEVS for proving a warm environment and answering all my questions and challenges. Thank you for sharing your experiences and knowledge thus making this thesis a success. My gratitude goes to Jonas Gunnarsson CDF engineer at NEVS for the introducing me to GT-SUITE modelling tool and your help in setting up my model. The rig team at NEVS Anders Nygren and Mats Johansson am really grateful for your assistance at the rig and measurements

Without Gamma Technologies support with licensing and orientation this thesis wouldn't have been possible, so many thanks them and to Brad Holcomb for answering all my modelling questions. Lastly i would like to thank my entire family for support, my wonderful husband Gerhard for continuously encouraging me.

Winnie Mwangi, Gothenburg, August 2018



# Contents

<b>List of Figures</b>	<b>1</b>
<b>List of Tables</b>	<b>1</b>
<b>1 Introduction</b>	<b>1</b>
1.1 Background . . . . .	1
1.2 Purpose . . . . .	2
1.3 Outline . . . . .	2
1.4 Scope . . . . .	2
<b>2 Theory of the thermal propulsion loop</b>	<b>3</b>
2.1 Heat Transfer Modes . . . . .	3
2.1.1 Conduction . . . . .	3
2.1.2 Convection . . . . .	3
2.1.3 Radiation . . . . .	5
2.2 Overview of the thermal propulsion loop . . . . .	5
2.2.1 Pump . . . . .	6
2.2.2 Radiator . . . . .	7
2.2.3 Fan . . . . .	7
2.2.4 Pipes and hoses . . . . .	8
2.2.5 Accumulator tank . . . . .	8
2.2.6 Power Electronics . . . . .	9
2.2.7 Electric machine . . . . .	9
2.2.7.1 Power Losses . . . . .	9
2.3 Coolant . . . . .	10
2.4 GT-SUITE Modelling . . . . .	11
2.4.1 Modelling interface in GT-SUITE . . . . .	11
<b>3 Modelling of the Propulsion Loop in GT-SUITE</b>	<b>13</b>
3.1 Pump . . . . .	13
3.2 Accumulator . . . . .	14
3.3 Radiator . . . . .	14
3.4 Pipes . . . . .	15
3.5 Power Electronic converters . . . . .	16
3.6 Fans . . . . .	16
3.7 Electric machine . . . . .	17
3.7.1 Thermal Modelling . . . . .	17

3.7.2	Electrical Modelling . . . . .	20
3.8	Simulated Case Set up . . . . .	23
3.9	Rig set up for measured copper losses . . . . .	25
<b>4</b>	<b>Results and Analysis</b>	<b>27</b>
4.1	Propulsion Loop Base Verification . . . . .	27
4.2	Steady state analysis at 4000rpm and 100Nm . . . . .	28
4.2.1	Base verification of the flow rate . . . . .	28
4.2.2	Simulated losses at 4000rpm 100Nm at different flow rates and coolant temperatures . . . . .	29
4.2.3	Temperature distribution in electric machines' parts . . . . .	30
4.2.3.1	Temperature distribution on EM parts @ 23deg coolant temperature . . . . .	30
4.2.3.2	Temperature distribution of EM parts @ 65deg coolant temperature . . . . .	31
4.3	Steady state analysis at 8000rpm 50Nm . . . . .	32
4.3.1	Electric machine parts temperature distribution at 8000rpm 50Nm . . . . .	33
4.3.1.1	Temperature distribution of EM parts @ 23 deg coolant temperature . . . . .	33
4.3.1.2	Temperature distribution of the EM parts @ 65 deg .	34
4.3.1.3	Electric machine parts temperature distribution at -10deg . . . . .	35
4.3.2	Comparison between losses at high speeds and low speeds . . .	36
4.3.3	Simulated, measured and manufacturers' copper losses . . . .	37
4.4	Pump power consumption . . . . .	38
4.5	Drive Cycle Operation . . . . .	39
4.6	Radiator dimension variation . . . . .	41
4.7	Fan signal point variation . . . . .	43
<b>5</b>	<b>Conclusion</b>	<b>45</b>
5.1	Future work . . . . .	45
	<b>Bibliography</b>	<b>47</b>

# 1

## Introduction

This chapter presents brief background and how the thesis will be outlined in the other chapters.

### 1.1 Background

Energy efficiency is a vital factor for technical systems operations and performance. Electric drives account for a big percentage of the electricity consumed. Efficient electric drives can improve technology to higher levels, lead less environmental impact and an overall cost reduction.

The electric motor is used widely in the electric vehicle industry and that is why they are the main target for significant energy savings, zero emissions and cost reductions.

The efficiency of an electric drive is influenced by power supply quality, inverter switching losses, electric machine efficiency, speed control and its' proper sizing. An electric drive has several components. It has a battery, a dc/dc converter, an inverter, an electric motor and connectors. The electric machine plays the major role.

The electric vehicle industry applications need electric machines that have high power density and high torque. For an electric machine to be able to meet this requirement, it has to spin at high speeds or be fed with high current density or a combination of both methods. High current density, leads to copper losses and high stator winding temperatures. As the rotor spins faster, it leads to high current and voltage, high frequencies, which in turn lead to higher iron losses in the stator and the rotor laminations.

In a permanent magnet machine it leads to high eddy current losses if the heat is not well dissipated. To reduce the losses in the electric drive system, optimization of the motor drive efficiency should be assessed. In this thesis, the thermal model of the propulsion motor will be modelled and losses will be assessed in the entire electric drive system.

### 1.2 Purpose

The purpose of this thesis was to model a propulsion thermal cooling loop of an electric vehicle and identify the main losses in the loop at different driving cycles, different ambient temperatures and flow rates, model a real prototype BEV and investigate energy saving potential.

The vehicle propulsion thermal cooling loop was tested in the National Electric Vehicle of Sweden (NEVS) Powertrain transmission laboratory. This thesis was thought to improve the losses in the propulsion loop and optimizing the entire cooling loop for energy efficiency of the electric drive.

This work will be performed with high consideration to facts and honesty. Data collected and generated will not be altered to suit a certain situation but suggestions can be made and will be clearly stated. This research is performed in order to investigate the main losses in an electric drive so as to improve its efficiency. High efficiency leads to high performance and contributes to better machines for society. Nowadays, an important incentive in the production of electric vehicles is for green driving and zero emissions since it contributes to less global warming and environmental hazards.

### 1.3 Outline

A CFD modelling tool is used to model the propulsion cooling loop. GT SUITE software was used to do the modelling. Different components on the loop were imported from CAD to the GT SUITE software and edited to be appropriate for modelling. GT SUITE tools such as SpaceClaim, GEM3D and GT Post were used.

In chapter 2, the theoretical overview of the components in the thermal loop is discussed in details. Chapter 3 covered the modelling of the loop in the CFD computer software. In chapter 4, analysis of the results will be done as well as base verification. Finally but not least in chapter 5 conclusion and future work was discussed.

### 1.4 Scope

In this study the radiator, fan, pump, accumulator and electric machine will be modelled in GT-SUITE in details as per its design. Manufacturers data sheets will be used as input during modelling. Power electronics will not be modelled into details but they will be used as heat sources.

# 2

## Theory of the thermal propulsion loop

### 2.1 Heat Transfer Modes

Heat is transferred in the thermal loop by different modes. These are conduction, convection and radiation. In this loop all modes of heat transfer are used. Some are used independently, some are used in combination.

#### 2.1.1 Conduction

This is the transfer of heat energy through solids, fluids and gases by collision of particles, molecules, atoms and electrons within a body. In an electric machine conduction occurs in its solid parts.

J.P. Holman [4] states that conduction is when the heat transfer rate  $q$  (W or J/s) is proportional to the thermal conductivity of a material ( $W/mK$ ), the temperature gradient in the direction of the heat flow  $\frac{\partial T}{\partial x}$  over the surface area  $A$  ( $m^2$ ), expressed as

$$q = -\lambda A \frac{\partial T}{\partial x} \quad (2.1)$$

The negative sign is inserted to fulfill the second principle of thermal dynamics. This equation is the Fourier law of heat conduction [4].

#### 2.1.2 Convection

This is the transfer of heat due to movement of molecules within fluids, gases and surfaces. On the surface, heat is transferred by conduction since the speed of the fluid is reduced to zero as a result of viscous action [4].

The temperature gradient is dependent on the volumetric flow rate that carries the heat away, thus convection. Newton's law of cooling is used to express the convection equation according to [4]

$$q = hA[T_w - T_\infty] \quad (2.2)$$

The heat transfer rate  $q$  (W) is proportional to the convection heat transfer coefficient  $h$  ( $W/m^2K$ ), the surface area of contact  $A$  ( $m^2$ ) by the temperature difference between

the wall and the surroundings.

If convection occurs unassisted, for instance by blower and fans, then it is called free or natural convection. If it is assisted then it is called forced convection. Natural convection in an electric machine occurs between the surrounding ambient air and the machine housing. The fins on a machine housing improve the surface area thus better transfer of heat. A forced convection is added by the use of a fan on the machine shaft.

For heavy loaded machines which require high power densities, for instance machines used for powertrain application, liquid cooling could be used. The cooling liquid media could be water, oil, glycol or a mixture combination and could be passed in the frame of the machine. Some machines have ducts inside the winding that could pass through oil for cooling. According to [5] forced convection in an electric machine also takes place in the air-gap as well as around the end winding.

As pointed out in [2][6] there are several factors that affect the convection of heat transfer: surface geometry, the nature of the fluid, the thermodynamic and transport properties of the fluid, and the flow rate. Thus the heat transfer by convection has to be empirically and experimentally determined.

The heat transfer coefficient is around 2-25  $W/m^2K$  for gases and 10-1000  $W/m^2K$  for liquids in natural convection and for forced convection it is 10-300  $W/m^2K$  for gases and 50-20,000  $W/m^2K$  for liquids [7][8][9]. A dimensionless Nusselt number  $Nu$  is used instead of a convection heat transfer coefficient. It is the ratio of conductive and convective heat transfer rates as described in [7],

$$\frac{q_{conv}}{q_{cond}} = \frac{hA\Delta T}{\frac{\lambda A\Delta T}{l_{thick}}} \quad (2.3)$$

(geometry,  $Re$ ,  $Pr$ )

where as  $l_c$  is the fluid layer length, the Nusselt number is dependent on geometry and two dimensionless parameters: the Prandtl number  $Pr$  and the Reynolds number  $Re$ . The former is defined as

$$Pr = \frac{C_p\mu}{\lambda} \quad (2.4)$$

where  $C_p$  (J/kgk) is the fluid specific heat capacity,  $\mu$  (kg/ms) is the dynamic viscosity and  $\lambda$  is the thermal heat conductivity according to [14]. In [7] and [10] the Prandtl number is described as a ratio of fluid momentum to heat diffusivity and it is only dependent on a medium's material parameter. Convective heat transfer takes place if  $Pr \gg 1$  and conductive heat transfer take place when  $Pr \ll 1$ .

Y.A sengel [11] has  $Pr$  for gases as 0.12-1, for water 1.12-13.7 and 50-10,000 for oils.

In [11] and [14] Reynolds number is described as the ratio of the fluid inertia to the viscous forces.

$$Re = \frac{\rho V l_c}{\mu} \quad (2.5)$$

where  $\rho$  ( $kg/m^3$ ) is the mass density,  $V$  ( $m/s$ ) is the fluid velocity,  $l_c$  is the characteristic length in ( $m$ ) and  $\mu$  is the dynamic viscosity in  $kg/m.s$ . Reynolds number determines the type of flow: for a high  $Re$ , a turbulent flow exists and for a low  $Re$  then a laminar flow exists. A transition from laminar and turbulent occurs at a defined or certain value of  $Re$  known as the critical Reynolds number [2]. That critical and specific number is affected by the type of fluid medium, surface geometry and roughness, temperature and surface. According to [2], it is difficult to predict these threshold analytically, but approximated values could be obtained from historically well-defined geometries and fluids.

### 2.1.3 Radiation

Radiation is a form of heat transfer in which electromagnetic waves or protons are emitted to colder surroundings according to [7] and [10]. Radiation is defined as

$$q_{rad} = \epsilon \delta A [T_w^4 - T_\infty^4] \quad (2.6)$$

where  $q_{rad}$  is the radiated heat transfer rate in (W),  $\epsilon$  is the surface emissivity,  $A$  is the surface area in ( $m^2$ ),  $T_w$  is the surface temperature in (K),  $T_\infty$  is the surrounding temperature and  $\delta$  is the Stefans-Boltzmann's constant which is  $5.6701 \cdot 10^{-8}$  ( $W/m^2 K^4$ ) [7]. The power of four is as found in Stefans-Boltzmann's equation when the emissivity and the absorbility of the compact body are equal, the transmission is then zero. Due to this, the heat exchange is dependent on radiation angles, emissivity and temperature of the interacting surfaces. The surrounding act as a black body when the absorbility is 1 [11].

Radiation is assumed negligible when there is a forced convection[7]. In [7] and [10] the heat transfer coefficient  $h_{rad}$  for radiation is stated as

$$q_{rad} = h_{rad} A [T_w - T_\infty] \quad (2.7)$$

where

$$h_{rad} = \epsilon \delta (T_w - T_\infty) (T_w^2 + T_\infty^2) \quad (2.8)$$

## 2.2 Overview of the thermal propulsion loop

In this particular investigation, the propulsion loop used for this study consists of a radiator, a fan, power electronics (inverter and dc/dc converter), a pump, pipes, coolant and an electric machine. There are also minor components such as an accumulator, air separator and on board charger. The coolant flows from the accumulator to the radiator, then to the power electronics and lastly to the

electric machine back to the radiator for cooling. Figure 2.1 is a model of the entire propulsion loop.

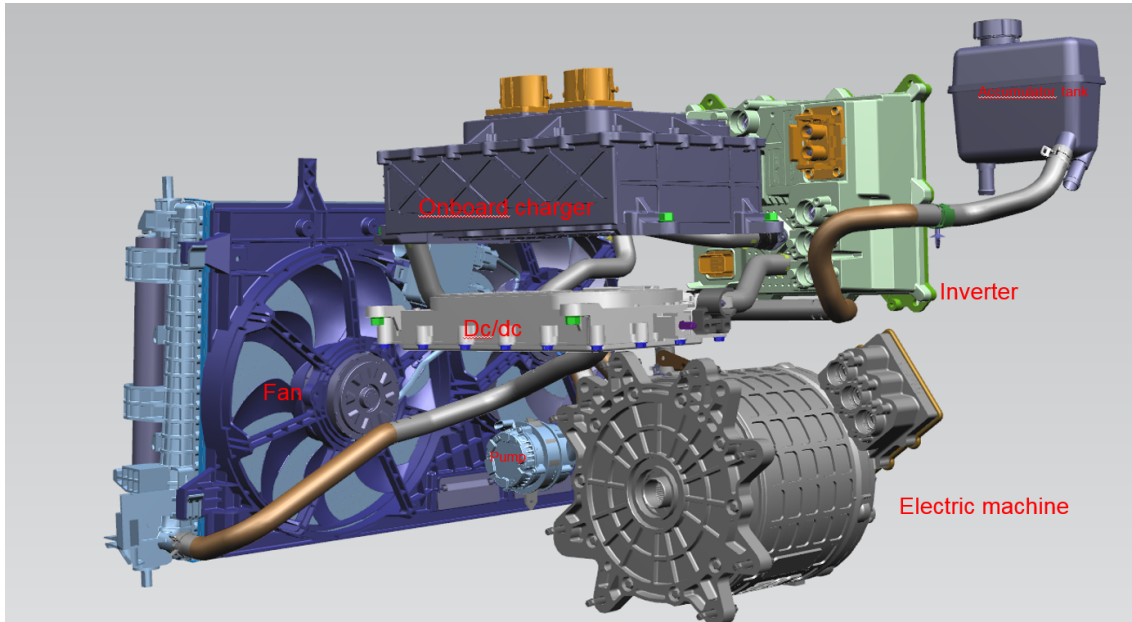


**Figure 2.1:** Propulsion loop in 3D graphics

### 2.2.1 Pump

The pump is used to pump the coolant through the cooling loop. It is controlled to adjust the flow rate depending on the temperature of the coolant. Due to the pressure drop generated in the pipes, the pump needs to put up enough pressure to overcome this drop. Mostly, a centrifugal pump is used and it converts the input power into kinetic energy by increasing the speed of the coolant in an impeller [12].

By Bernoulli equation, pumps can transfer input into kinetic energy. The impeller accelerates as described by the affinity laws whereby a fast rotating impeller will increase the speed of the coolant. An electric machine drives the impeller.

The pump used in this cooling loop is an electric pump with an electronic control system that adjusts the flow rates depending on the temperature information. An example of an electric pump is shown in figure 2.2 below



**Figure 2.2:** Electric pump for the propulsion loop [13]

### 2.2.2 Radiator

The radiator exchanges heat between the air in front of the car and the cooling loop. Most radiators consist of inlet and outlet tanks and a core. The core is made of thin aluminum tubes with fins that increase the rate of heat transfer to the atmosphere. The core is the main area where heat exchange occurs in a radiator.

The tanks are placed on the sides of the core. For horizontal radiators, the tanks are placed on the sides and the aluminum tubes run along horizontally. For vertical radiators, the tanks are placed at the top and the bottom of the core with tubes running vertically. Pipes feed the tanks with the coolant. Examples of radiators is shown in the figures 2.3 and 2.4.



**Figure 2.3:** Horizontal model [14]



**Figure 2.4:** Vertical model [14]

### 2.2.3 Fan

Fans are mostly placed on the inside of the radiator, allowing air to flow into the radiator directly leading to an improved performance, see figure 2.5. A fan is supposed to enhance the air circulation all the time the vehicle machine is running, for

instance at low speeds or at standstill.

The temperature sensor information is sent into the electronic controls and depending on this information, the controls will send a signal to the fan to turn on or not.



**Figure 2.5:** Electric fan for the propulsion loop [15]

### 2.2.4 Pipes and hoses

Pipes and hoses are the transport means of the coolant through the entire loop. They also connect the components in the propulsion loop. They are designed to withstand fluid dynamics such as different pressure and temperatures depending on the operating situations. See figure 2.6 for example of pipes used in a cooling loop.

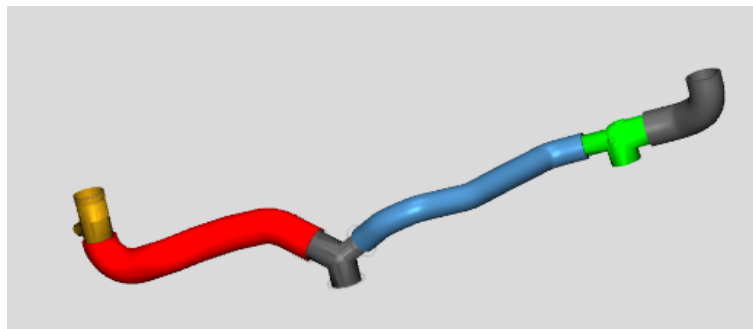


**Figure 2.6:** Pipes

### 2.2.5 Accumulator tank

Once the coolant gets hot, it expands and the accumulator tank, see figure 2.7, will accommodate the expanding coolant, via pressure valve.



**Figure 2.7:** Accumulator tank [16]

## 2.2.6 Power Electronics

There are two power electronic converters in this loop: an inverter and a dc/dc converter. A dc/dc converter is used to convert the unregulated dc input into controlled dc output at a desired voltage level [1]. In the automotive industry, the dc/dc converter allows energy transfers between the high voltage battery and the 12 volts systems.

An inverter according to [1] is used in an electric drive with the objective to produce a sinusoidal ac output with a magnitude and frequency that can be controlled. Switching devices are the main causes of losses in power electronic converters. Two IGBT switches that are connected in parallel and a freewheeling diode make a switch [2]. The main losses in power electronic converters are switching and conduction losses.

## 2.2.7 Electric machine

The electric machine in this thesis is a PMSM.

### 2.2.7.1 Power Losses

The main losses in a PMSM are copper losses, iron losses and windage. Copper losses are also known as resistive losses and are a result of current passing through the copper winding. Iron losses are composed of stator core losses and rotor core losses.

Copper losses are affected by the number of phases of the current, the copper winding resistance and the RMS value of the phase current. Therefore copper losses can be calculated as

$$P_{cu} = 3R_s I_s^2_{RMS} \quad (2.9)$$

The  $I_s$  RMS in a dq frame is expressed as [2]

$$I_s = (I_d^2 + I_q^2) \quad (2.10)$$

From equation (2.13) copper losses can be calculated by

$$P_{cu} = 3R_s(I_d^2 + I_q^2) \quad (2.11)$$

Stator resistance affect the copper losses since resistance is temperature dependent such that

$$R_s = R_0[1 + \alpha(T - T_0)] \quad (2.12)$$

where  $R_s$  is the copper winding resistance,  $R_0$  is the initial resistance value,  $\alpha$  is the temperature coefficient of copper and  $T_2$  is the temperature after the winding is heated. It is possible to estimate the copper winding temperature after the winding has been heated up. This can be done by the following equation according to [11]

$$T_2 = \frac{R_2}{R_1}(234.5 + T_1) - 234.5 \quad (2.13)$$

Where  $T_2$  is the temperature of the winding,  $T_1$  is the ambient temperature,  $R_0$  is the winding resistance initial value and  $R_2$  is the winding resistance value after the winding has heated up. The winding resistance may also be affected by the frequency of the supply voltage through the skin effect or the proximity effect [2].

Iron losses are related to the physical components and material characteristics. They are influenced by the magnetic hysteresis and induced eddy currents. According to [2] the iron losses can be expressed as

$$P_{fe} = K_h f B_{pk}^n + K_c f^2 B_P K^2 \quad (2.14)$$

Where  $K_h$  is the hysteresis parameter,  $f$  is the frequency of the flux,  $B_{pk}$  is the peak flux density in the  $B-H$  hysteresis curve,  $K_c$  is the eddy current parameter and  $n$  is dependent on  $B_P K f_r$  and the steel material. In each operation, energy is lost in the core materials in  $B-H$  loop which causes hysteresis losses. It is directly dependent on the frequency of operation, therefore it is difficult to estimate [2]. Eddy current losses can be reduced by using thinner laminations.

The thermal model of a PMSM can be done in several ways such as lumped parameter modelling, CDF and FEA software. FEA and CDF are typically implemented in computer software where overall temperature distribution can be obtained in a computer simulation. They analyze detailed geometries according to preferences. In lumped parameters, a motor is segmented into several components and each component is presented by a node.

### 2.3 Coolant

Coolant is a liquid used in the cooling system, the radiator and the electric machine of an electric vehicle or combustion engine vehicle. Some ingredients such as

ethylene glycol or propylene glycol are added to the coolant water to keep it from freezing during winter and boiling during summer [17].

It also acts as a lubricant to the entire cooling system. Common mixtures of the antifreeze and water are 50:50, 40:60 or 20:80. Coolants with lower antifreeze usually have lower viscosity which leads to lower Resistance and less load on the pump [17]. According to [17] such liquids should be used in cold conditions.

The coolant transfers heat using the heat transfer formula

$$Q = mc\Delta T \quad (2.15)$$

where  $Q$  is the heat content in Joules,  $m$  is the mass,  $c$  is the specific heat in  $J/Kg-K$ ,  $T$  is the temperature and  $\Delta T$  is the change in temperature.

The coolant used in the loop is a water/glycol mixture of 50/50 with a specific heat capacity of 3300J/Kg-K.

## 2.4 GT-SUITE Modelling

### 2.4.1 Modelling interface in GT-SUITE

GT-SUITE is a CFD 1D software from Gamma Technologies that is used for modelling, simulating and analyzing various multiphysics engineering aspects. The GT-suite provides different applications as shown in Figure 2.9.

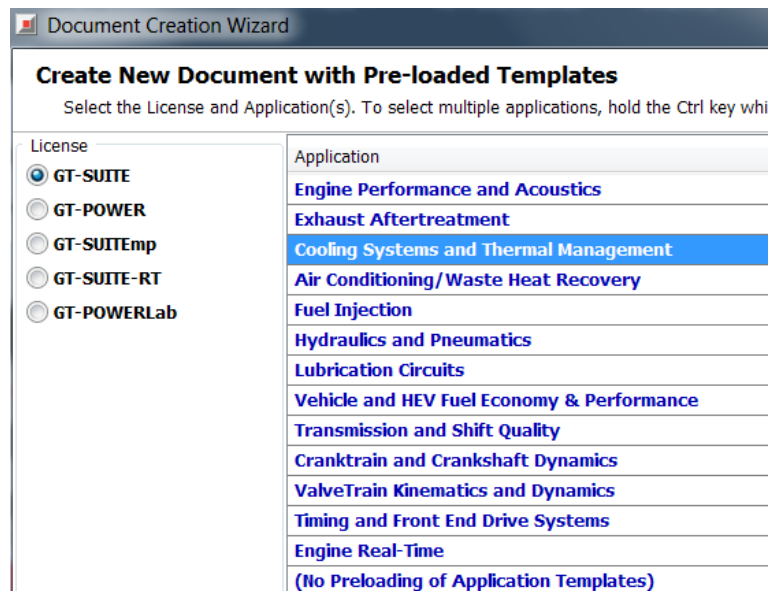
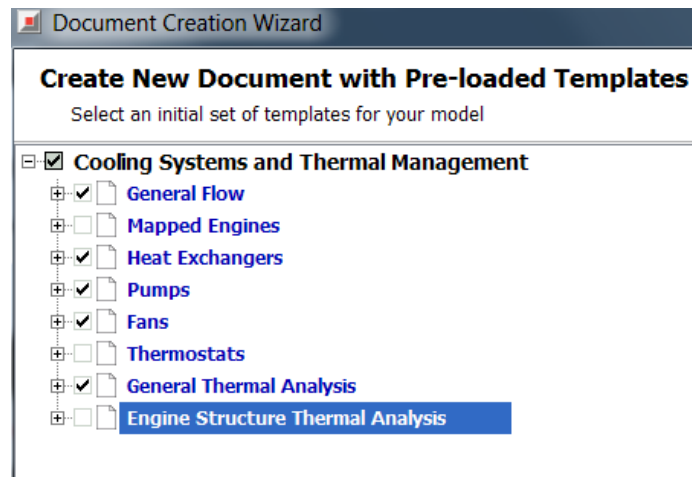


Figure 2.8: GT-SUITE modelling template

In this thesis, cooling system and thermal management is used. Figure 2.10 shows the components inside the cooling system and thermal management in GT-SUITE.



**Figure 2.9:** GT-SUITE cooling systems and thermal management template

GT-SUITE has various operating tools such as GT-ISE, GEM3D, COOL3D, VTDesign, GT-Spaceclaim and GT Post. In this study, GEM3D, GT-Post, GT-Spaceclaim and GT-ISE are used.

GEM3D is a preprocessor that builds and imports 3D components which can be converted 1D GT-SUITE models. GT-Spaceclaim is a 3D CAD tool that imports and converts to GEM3D or GT-ISE. In spaceClaim editing can be done to desired geometries as well.

# 3

## Modelling of the Propulsion Loop in GT-SUITE

The propulsion loop was modelled as shown in figure 3.1, illustrated by the purple line. Each component was modelled separately in the GT-SUITE modelling tool.

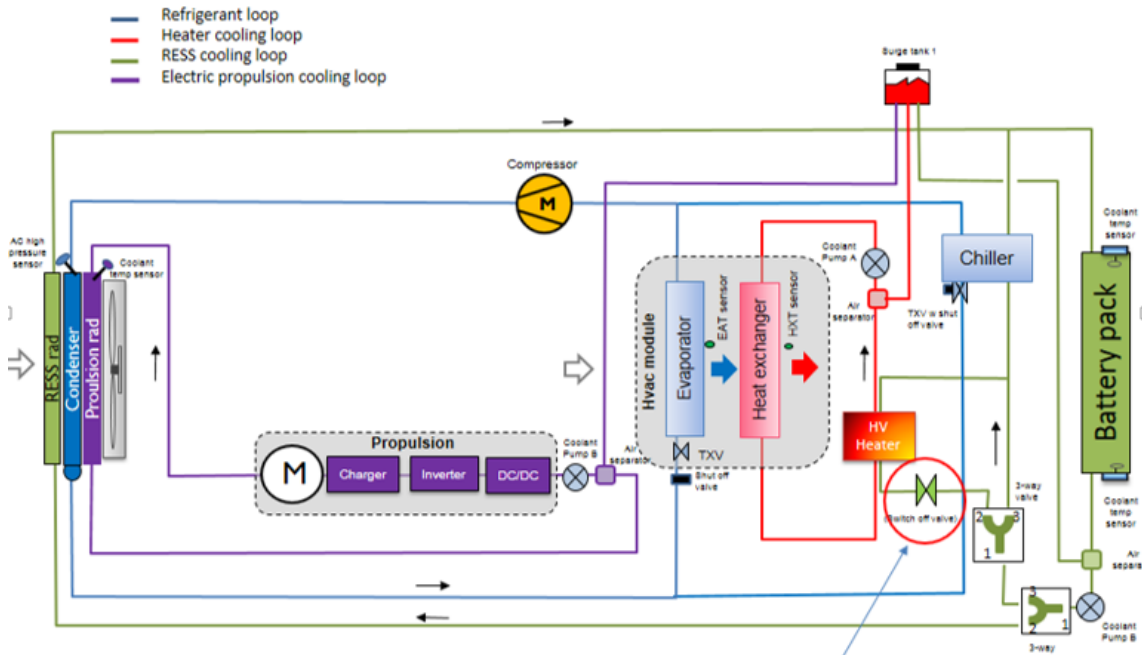
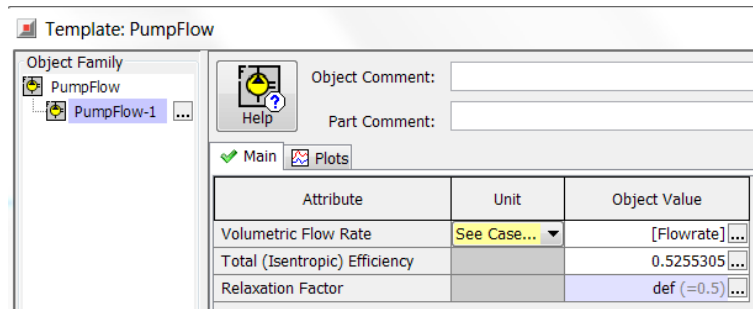


Figure 3.1: Cooling loop schematic diagram

### 3.1 Pump

The coolant pump was modelled by a pump object from the GT-SUITE library. The performance data of the pump is documented in the NEVS corporate data base. This data include the size of the pump, speed in rpm, efficiency and power. The data used was provided by the manufacturer. The pump model chosen in this study was such that efficiency was kept constant. The Figure 3.2 shows the efficiency of the pump used during modelling.



**Figure 3.2:** Pump efficiency

The flow rate used for this study was 3 l/min, 6 l/min and 12 l/min. The pump was set to pump these three flow rates and its energy consumption was analyzed in relation to its cooling efficiency.

## 3.2 Accumulator

The accumulator or expansion tank, see Figure 3.3, was modelled in GT-SUITE using an accumulator component found in the flow. The tank capacity used was 1.8 litres. The pressure was set so that a vacuum was not created in the accumulator.

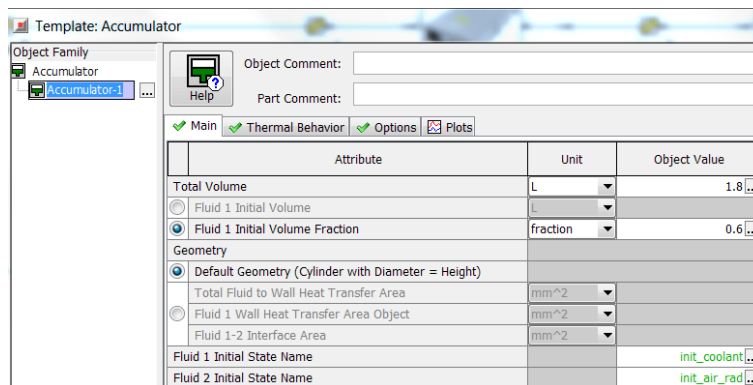


**Figure 3.3:** Modelling properties of Accumulator tank

## 3.3 Radiator

The radiator was defined using master and slave objects in GT-SUITE, see Figure 3.4. The master was connected to the coolant side of the loop while the slave was connected to the air side of the loop. Data of its size and performance was provided by the manufacturer and documented in the NEVS corporate database. In this study, the size of the radiator was altered in GT-suite to investigate how that affects the cooling of the electric machine.

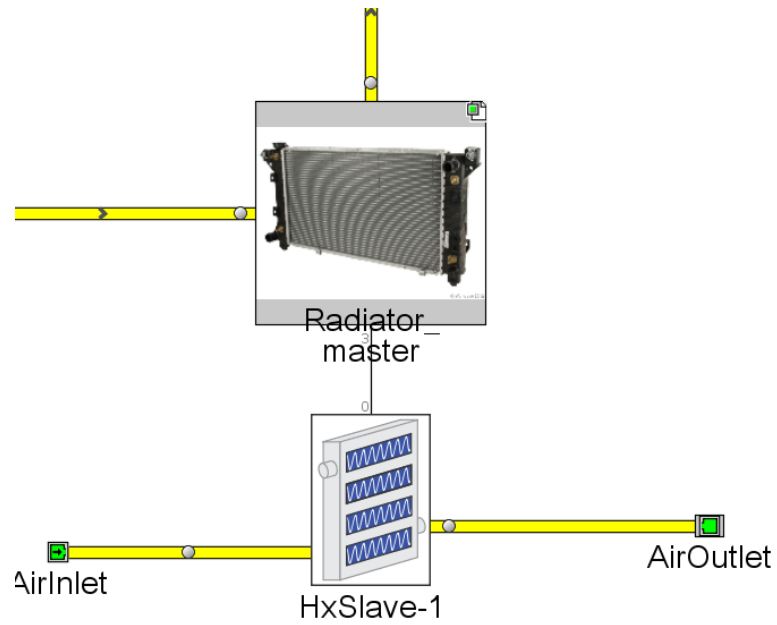


**Figure 3.4:** Radiator master and slave

## 3.4 Pipes

The pipes CAD model was imported to GT-SpaceClaim and the sizes of the pipes were edited to suit the project. This CAD model is used in the prototype car used in this thesis study. They were then imported to GEM3D and the pipes were converted to components and allocated volume. In GEM3D, the pipes are as shown in figure 3.5.

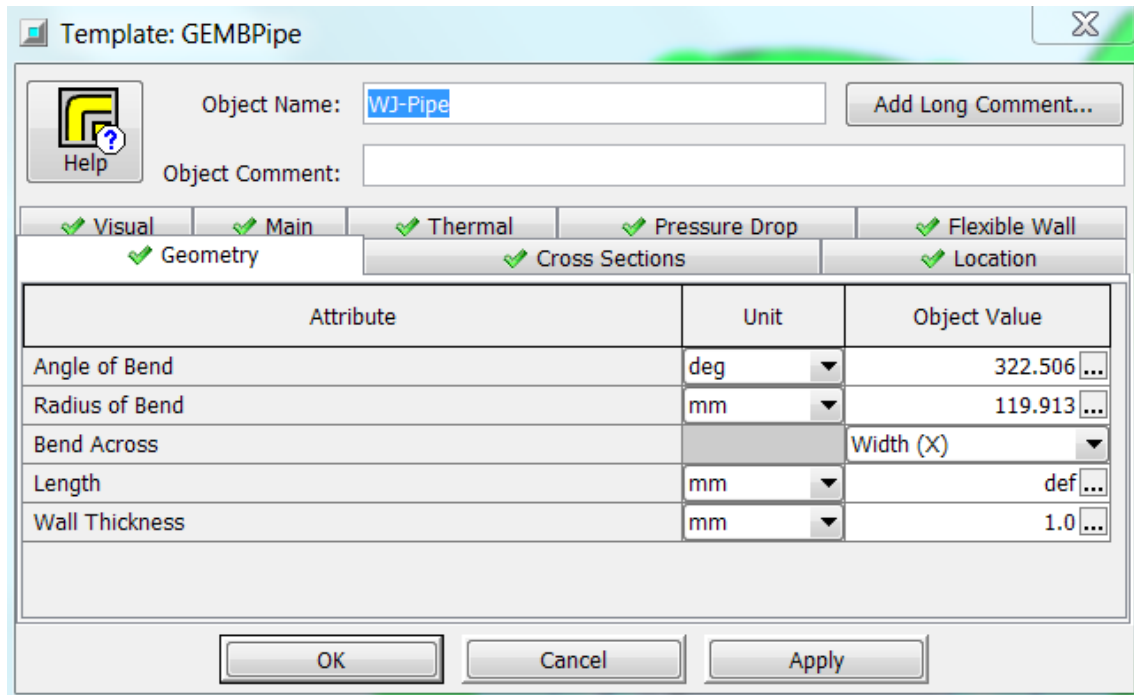


Figure 3.5: Pipes editing in GEM3D

## 3.5 Power Electronic converters

The power electronic converters were modelled as heat sources since the manufacturer's data was missing. A constant heat source of 500 watts was allocated to them.

## 3.6 Fans

The fan was modelled as an electric fan with its data filled up in an XYZ input map. This data include the fan size, its efficiency, speed and power. In the prototype car, there are two fans but in this thesis the data of both fans was combined and modelled as one. This particular fan turns on when the coolant temperature reaches 60 deg and slowly accelerates with increasing coolant temperature. The fan rotates at full speed when the temperature reaches 65 deg. The power consumption of the fan was investigated. Figure 3.6 shows the fan signal which the trigger to the fan.

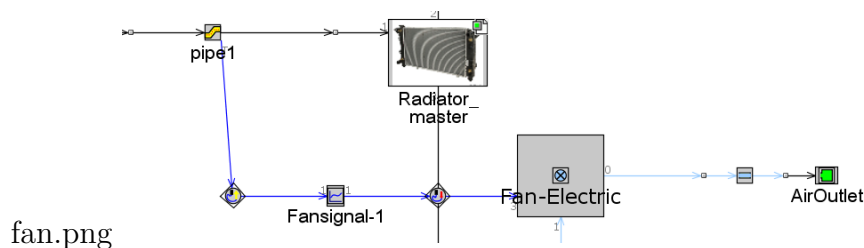
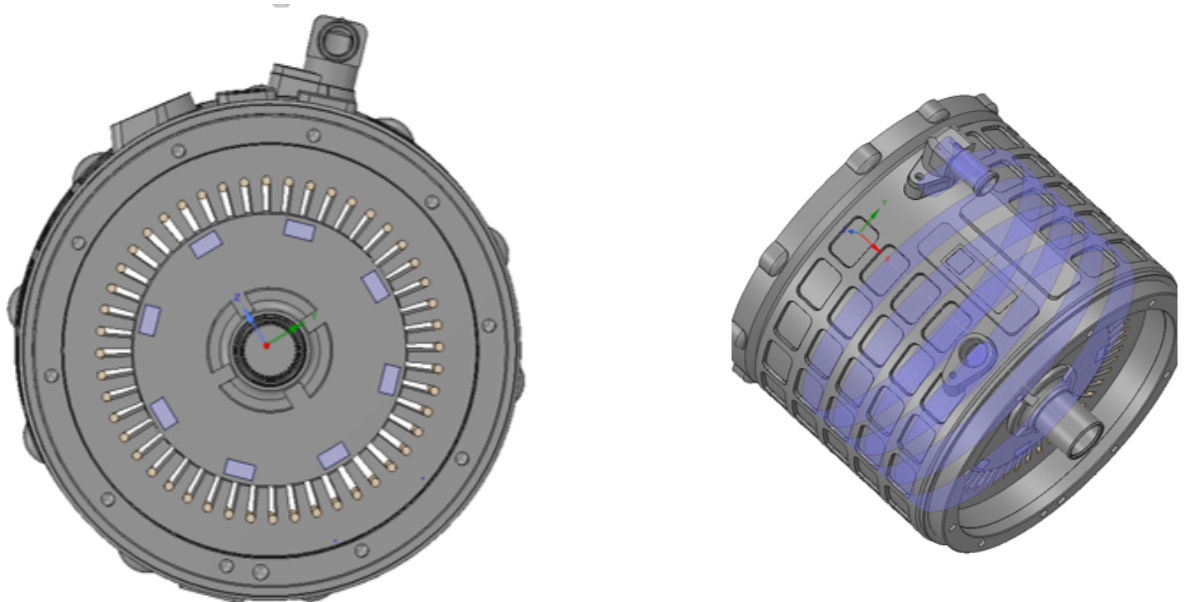


Figure 3.6: Electric fan in GT-SUITE modelling

## 3.7 Electric machine

### 3.7.1 Thermal Modelling

The electric machine CAD model was imported to SpaceClaim. In the SpaceClaim environment, the motor geometry was edited to suit the desired modelling. A volume was extracted from the electric machine using a volume extract tool. This created a water channel for the cooling fluid. Figures 3.7 and 3.8 show the SpaceClaim CAD import and an extracted volume inside the electric machine.



**Figure 3.8:** Extracted volume

**Figure 3.7:** CAD import of EM in GT-spaceClaim

In this particular CAD geometry, the stator and the water jacket were designed as one component, so using a splitting spaceClaim tool the stator and water jacket were separated. This was done to allow allocation of different materials to the stator and water jacket.

Then the entire geometry was imported to GEM3D see Figure 3.8 In GEM3D the electric machine parts were converted into components and the material properties were specified.

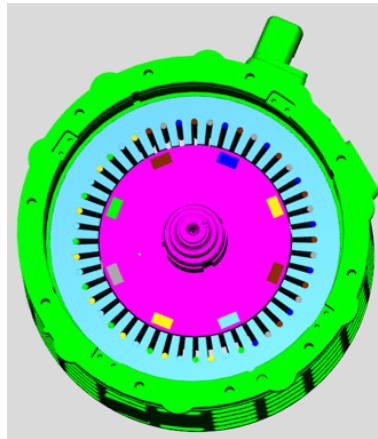


**Figure 3.9:** Electric machine import to GEM3D

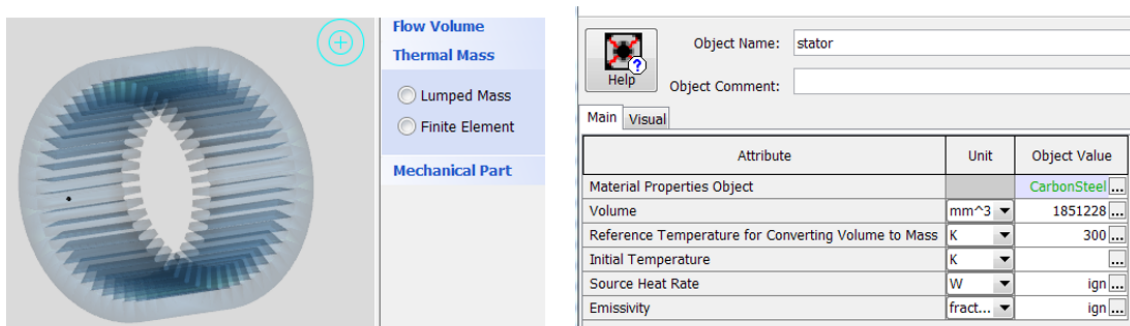


**Figure 3.10:** Converting EM parts to components and material properties allocation

In this tool, the name of the machine parts and its volume was stated but the volume and geometry was automatically calculated from the CAD import.

The material properties for winding was copper, stator and rotor was laminated carbon steel and the shell was aluminum. Most of the materials properties were already in GEM3D except for that of magnet. Its material properties were filled in manually as shown in figure 3.11.

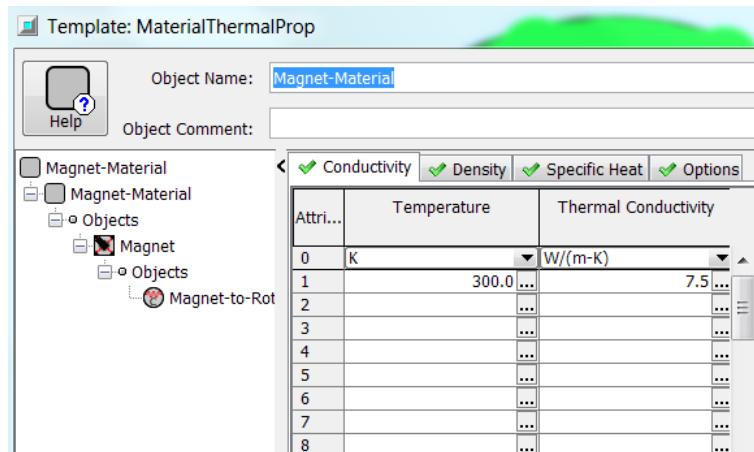


**Figure 3.11:** Magnet material allocation in GEM3D

The machine parts were converted into GEM3D components either as flow volume, mechanical parts or thermal masses. The flow volume was used for pipes and water jackets. With thermal mass there is an option of modelling the components as lumped models or finite elements. In this thesis a lumped model was used for stator, rotor, winding, magnets and shell.

The electric machine in this study has eight magnets but only one was converted and its volume multiplied by eight. The same applies for the winding one winding was converted and its volume multiplied by forty eight. Water jackets were converted into pipe splits through flow volume option. For pipes with right angles, a flow split was used and for the rest flow pipes. Figure 3.12 shows machines parts converted into thermal masses.

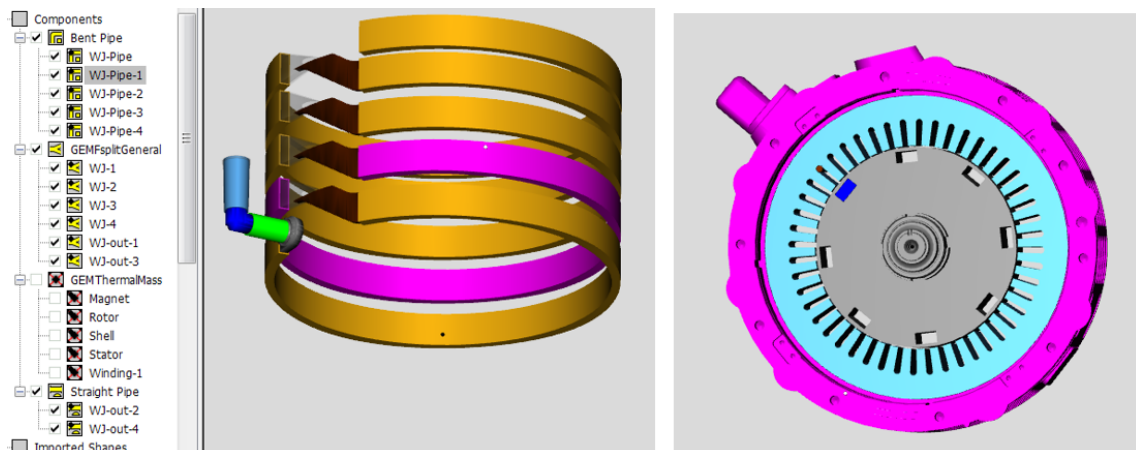


**Figure 3.12:** EM parts converted to thermal masses in GEM3D

A convection connection was added between shell and water jacket pipe as well as between flow split and shell. The thermal conductance connection was added between magnet and rotor, rotor and stator, stator and shell and between winding and stator. The model was imported to GT-ISE shown in figure 3.13.

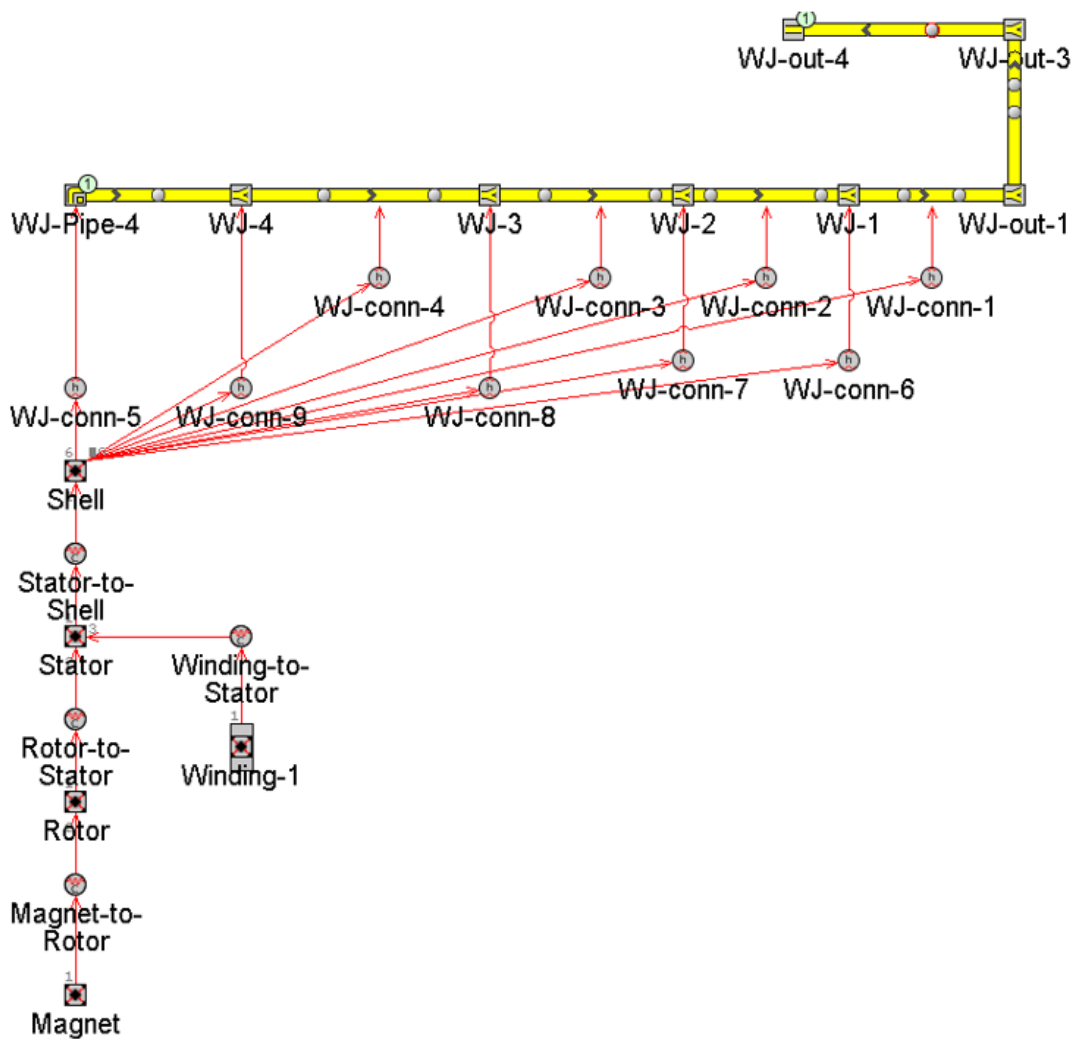


Figure 3.13: Thermal model of EM.

### 3.7.2 Electrical Modelling

The losses of the electric machine were to be investigated and how the cooling affects them. The copper and iron loss data were provided from the manufacturer as a function of speed and torque.

Speed and torque functions were added as signal generators. These signal generators have an input of speed and torque. Speed and torque input was for both dynamic and steady state operation properties. A speed of 4000rpm with 100Nm and 8000rpm with 50Nm was used as steady state operation and the WLTC drive cycle was used for dynamic operation.

2D look up table were used to collect phase current data as a function of speed and torque in combination with math operations. Using (2.16) a math function was implemented that updated resistance due to temperature changes. This resistance

was an input to a copper loss math function which used (2.15). A XYZ map of torque and speed was used in combination with the 2D look up table to give total copper losses as ()as shown in figures 3.14 and 3.15.

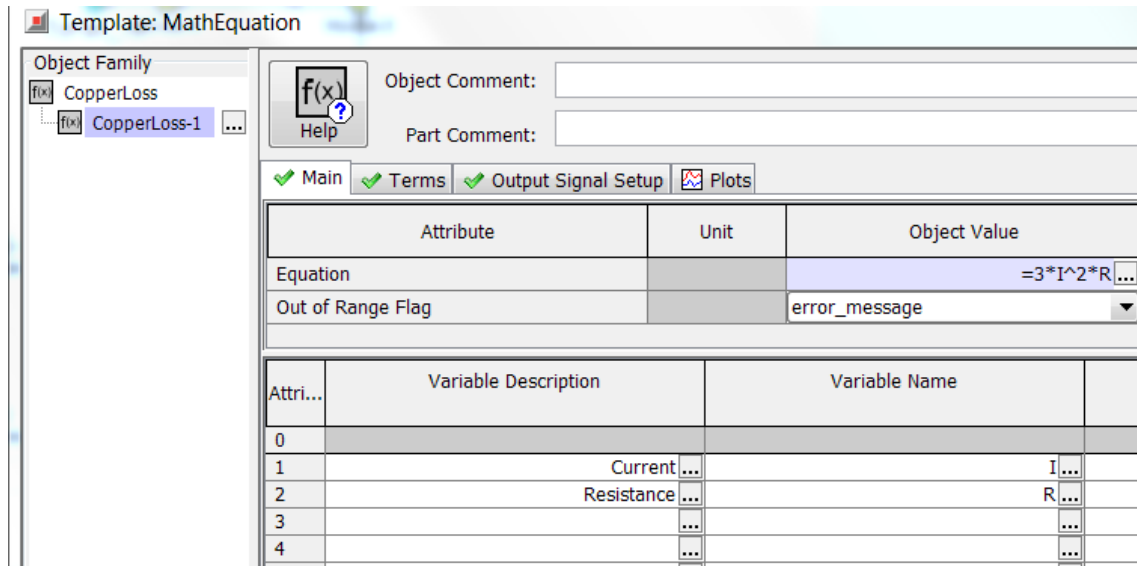


Figure 3.14: Copper losses realization.

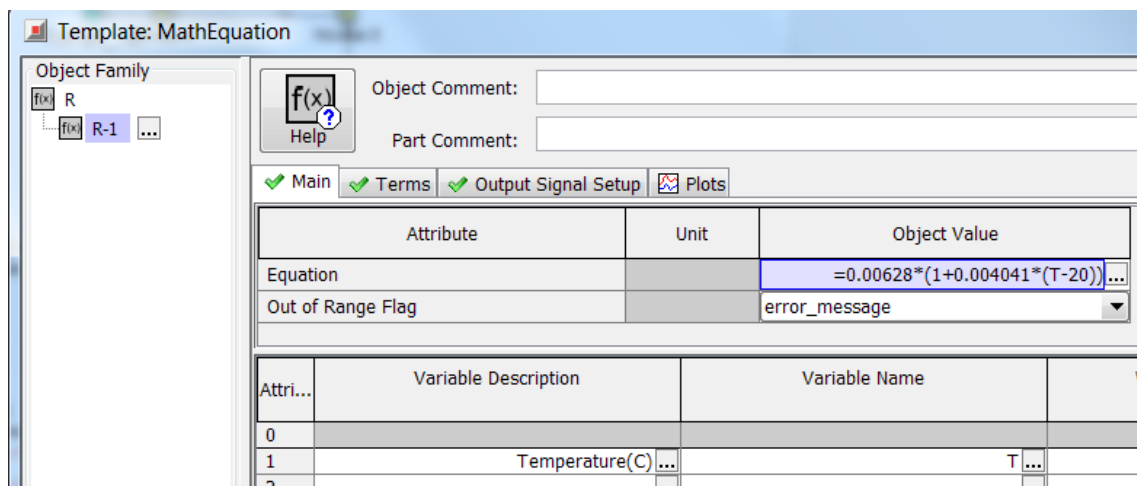


Figure 3.15: Resistance math function.

Once the electrical part is modelled, then the modelling is done and the electric machine can be used as desired. The complete model is shown in Figure 3.16

### 3. Modelling of the Propulsion Loop in GT-SUITE

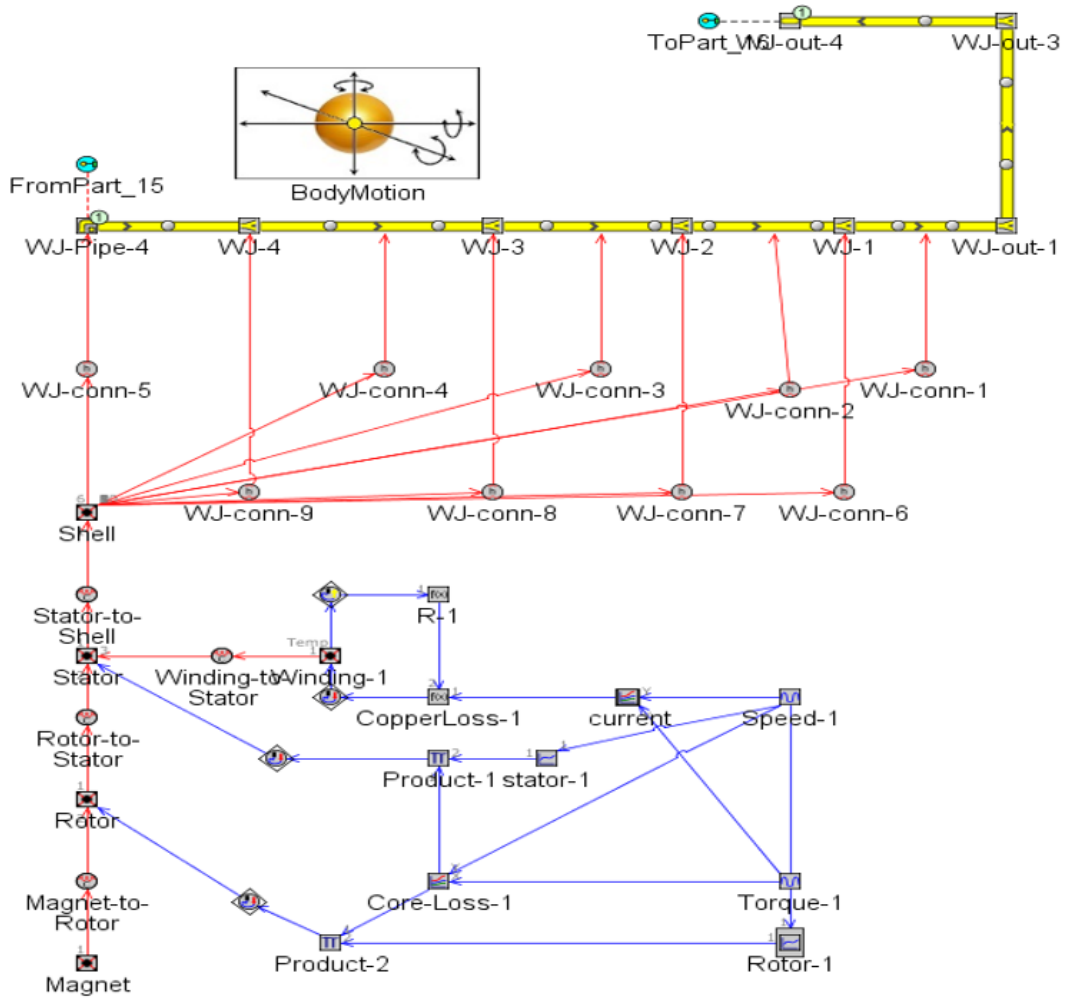


Figure 3.16: Complete model of EM

With pipes and the rest of components in place the propulsion loop was as shown in Figure 3.17.

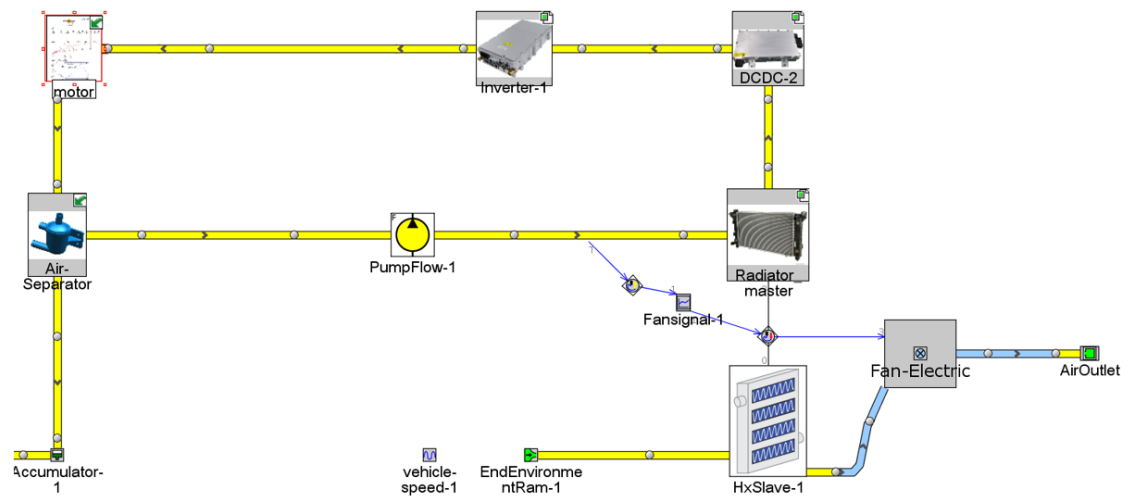


Figure 3.17: Complete propulsion loop

### 3.8 Simulated Case Set up

Various flow rates and coolant temperatures were studied. How they affect the losses on the machine and machine parts was also observed. The coolant temperatures considered were -10 degrees for winter conditions, 23 deg for normal summer weather in Sweden and 65 deg as extreme case. The flow rates were 3l/min, 6l/min and 12l/min.

Different sizes of the radiators were also observed and how they affect the cooling of the entire loop. The pump and fan power consumption were analyzed in GT-post in various combination of operation and change in energy consumption was noted. Loss distribution was also analyzed using WLTC drive cycle. The complete case set up was as shown in Figure 3.17.

### 3. Modelling of the Propulsion Loop in GT-SUITE

Parameter	Unit	Description	Case 1	Case 2	Case 3	Case 4	Case 5	Case 6	Case 7	Case 8	Case 9
Case On/Off		Check Box to Turn Case On	<input checked="" type="checkbox"/>								
Case Label		Unique Text for Plot Legends	Flat top speed ...								
DCDC_hestrate	W	Heat Input Rate	0 ...	0 ...	0 ...	0 ...	0 ...	0 ...	0 ...	0 ...	0 ...
Inverter_hestrate	W	Heat Input Rate	0 ...	0 ...	0 ...	0 ...	0 ...	0 ...	0 ...	0 ...	0 ...
init_air_temp	C		23 ...	23 ...	23 ...	65 ...	65 ...	65 ...	-10 ...	-10 ...	-10 ...
init_coolant_temp	C		23 ...	23 ...	23 ...	23 ...	23 ...	23 ...	-10 ...	-10 ...	-10 ...
init_coolant		Initial State Name	init_coolant ...								
init_wall_temp	C		23 ...	23 ...	23 ...	65 ...	65 ...	65 ...	-10 ...	-10 ...	-10 ...
init_air		Gas/Vapor Initial State Name	init_air_rad ...								
init_temp	C	Initial Temperature	23 ...	23 ...	23 ...	65 ...	65 ...	65 ...	-10 ...	-10 ...	-10 ...
multiplier		Heat Transfer Multiplier	1 ...	1 ...	1 ...	1 ...	1 ...	1 ...	1 ...	1 ...	1 ...
Distance	mm	Distance to Mass Center	11.5 ...	11.5 ...	11.5 ...	11.5 ...	11.5 ...	11.5 ...	11.5 ...	11.5 ...	11.5 ...
torque		Constant or Dependency Refer...	Torque								
speed		Constant or Dependency Refer...	speed								
smallheight	mm	Heat Exchanger Height	398 ...	199 ...	265 ...	398 ...	398 ...	398 ...	398 ...	398 ...	398 ...
smallwidth	mm	Heat Exchanger Width	650 ...	325 ...	433 ...	650 ...	650 ...	650 ...	650 ...	650 ...	650 ...
Flowrate	L/min	Volumetric Flow Rate	3 ...	6 ...	12 ...	3 ...	6 ...	12 ...	3 ...	6 ...	12 ...

Figure 3.18: Simulation case set up

### **3.9 Rig set up for measured copper losses**

A measurement was done in the rig for copper loss of the electric machine. The inverter provided phase currents as a function of torque and speed. The electric machine temperature in the winding was monitored by a sensor. Using sensor data on (2.12), the winding resistance was collected. This resistance data was then used on (2.9) to obtain copper loss of the machine.



# 4

## Results and Analysis

### 4.1 Propulsion Loop Base Verification

A base verification was done on the loop to ensure that the loop was operating as it should. All the components were set to have zero constant heat sources except for the electric machine that was used for verification.

The electric machine was fed with a constant heat source of 353W, which was a calculated figure from the heat transfer formula (2.15).

The flow rate was set to be 6 l/min which is 0.107kg/s mass flow rate. A delta T of 1 deg is expected from a 353W heat loss with 6 l/min flow rate. The figure 4.1 shows that the propulsion loop is working as expected. Temperatures increased by 1 deg from 23.3 deg to 24.3 deg after the coolant passed through the electric machine heat source of 353 watts. The cooling loop is operating as expected.

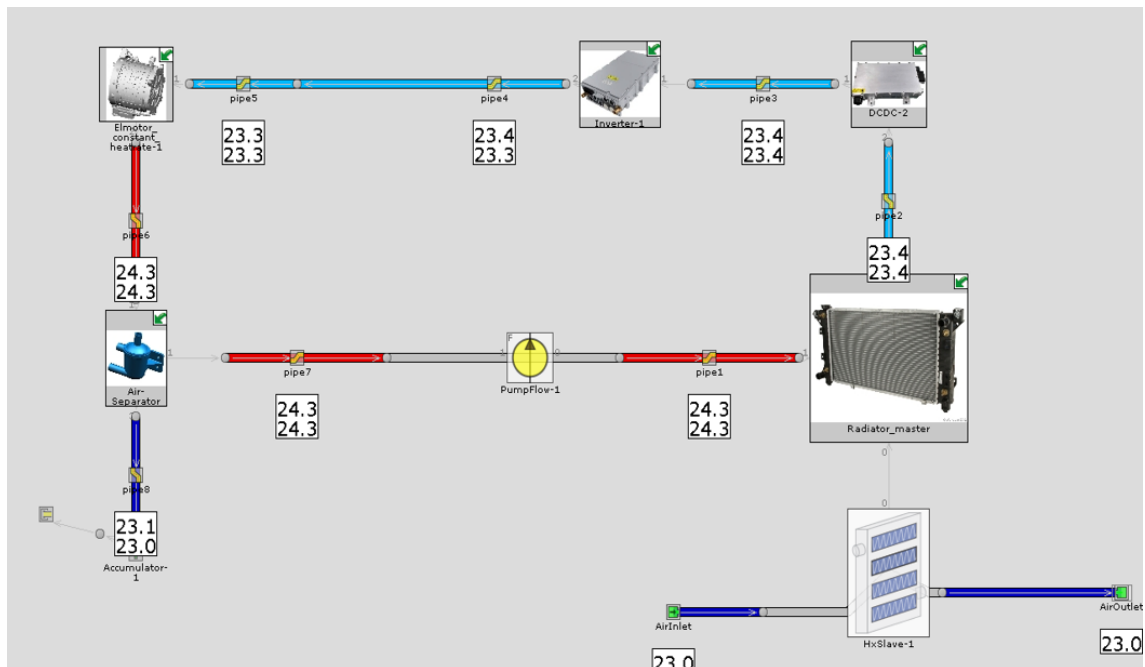


**Figure 4.1:** Propulsion loop base verification loop

Temperatures increased by 1 deg from 23.3 deg to 24.3 deg after the coolant passed through the electric machine heat source of 353 watts. The cooling loop is operating

as expected.

## 4.2 Steady state analysis at 4000rpm and 100Nm

The electric machine was set to run at 4000rpm with 100Nm torque at different coolant temperatures and flow rates. Electric machine losses and the pump power consumption were investigated.

### 4.2.1 Base verification of the flow rate

The flow rates were verified by both calculation and simulation using (2.13). This is to ensure the pump is pumping requested flow rates. The table 4.1, 4.2 and 4.3 show calculated and simulated delta T figures of different flow rates and coolant temperatures.

**Table 4.1:** Flow rates base verification @ 23deg coolant temperature

<b>Flow rate</b> <i>l/min</i>	<b>Calculated</b> <i>deg</i>	<b>Simulated</b> <i>deg</i>	<b>Diff</b>
3	8.53	8.55	0.02
6	3.96	3.98	0.02
12	1.96	1.99	0.03

**Table 4.2:** Flow rates base verification @ 65deg coolant temperature

<b>Flow rate</b> <i>l/min</i>	<b>Calculated</b> <i>deg</i>	<b>Simulated</b> <i>deg</i>	<b>Diff</b>
3	8.54	8.49	0.05
6	4.2	4.19	0.01
12	2.09	2.11	0.02

**Table 4.3:** Flow rates base verification @ -10deg coolant temperature

<b>Flow rate</b> <i>l/min</i>	<b>Calculated</b> <i>deg</i>	<b>Simulated</b> <i>deg</i>	<b>Diff</b>
3	8.10	8.09	0.01
6	4.01	4.02	0.01
12	2.0	2.1	0.1

The difference in the flow rates delta T between calculated and simulated figures, in all operating coolant temperatures is quite small. This means that the pump is pumping the requested flow rates.

### 4.2.2 Simulated losses at 4000rpm 100Nm at different flow rates and coolant temperatures

A steady state simulation was done with 4000rpm and 100Nm and simulated losses were as for Figure 4.2 and table 4.4.

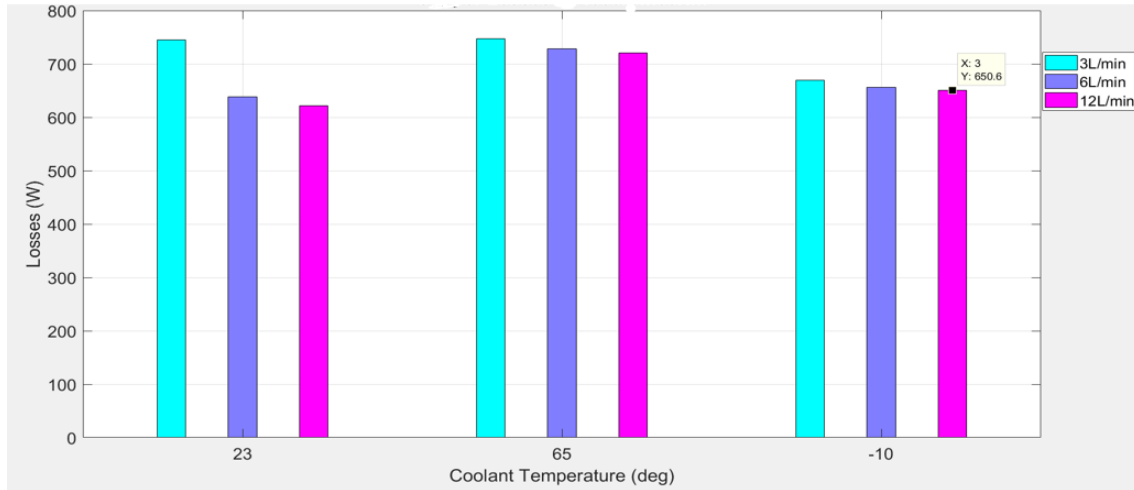


**Figure 4.2:** Simulated copper losses at 4000rpm 100Nm

**Table 4.4:** Simulated losses at 4000rpm 100Nm.

Flow rate <i>l/min</i>	P <sub>cu</sub> <i>W</i>	P <sub>cu</sub> <i>W</i>	P <sub>cu</sub> <i>W</i>
—	23	65	-10
3	745.2	747.3	669.4
6	638.1	728.9	656.6
12	621.5	720.2	650.6

The simulated copper losses increase with a decrease in flow rate and were high when the coolant temperature was high, at 65 deg. When the flow rate was reduced, the motor was not sufficiently cooled. The resistance in the copper winding increased thus leading to an increase in copper losses. Iron losses were 761 watts and remained constant at this specific speed and torque in all coolant temperatures. The iron losses are caused by magnetic hysteresis and eddy currents. These two properties are temperature dependent but here it is ignored thus at this speed and torque the iron losses remained constant.

At -10 degrees coolant temperatures, 6l/min flow rate, the losses are higher than for the same flow rate at 23 degrees. This could be because of the fluid dynamics changes. The viscosity of the coolant increases and it get more resistant to flow. The coolant becomes thicker and heavy to be pumped sufficiently thus leading to poor cooling and increase in temperature in the electric machine parts leading to high losses.

### 4.2.3 Temperature distribution in electric machines' parts

Motor winding temperature was calculated and compared to the simulated winding temperatures using (2.13) and were as for table 4.5. The calculated and simulated

**Table 4.5:** Winding temperatures base verification @ 23deg coolant temperature

Flow rate <i>l/min</i>	Calculated <i>deg</i>	Simulated <i>deg</i>	Diff
3	94.2	91.95	2.25
6	47.15	46.08	1.07
12	39.94	38.95	0.99

winding temperature difference is acceptably small. This shows that the model is responding to temperature change as it should.

#### 4.2.3.1 Temperature distribution on EM parts @ 23deg coolant temperature

The electric machine was operated at steady state 4000rpm 100Nm and temperature in its parts was investigated. At 23 deg coolant temperature the machine heated up as shown in Figure 4.3 and Table 4.6.

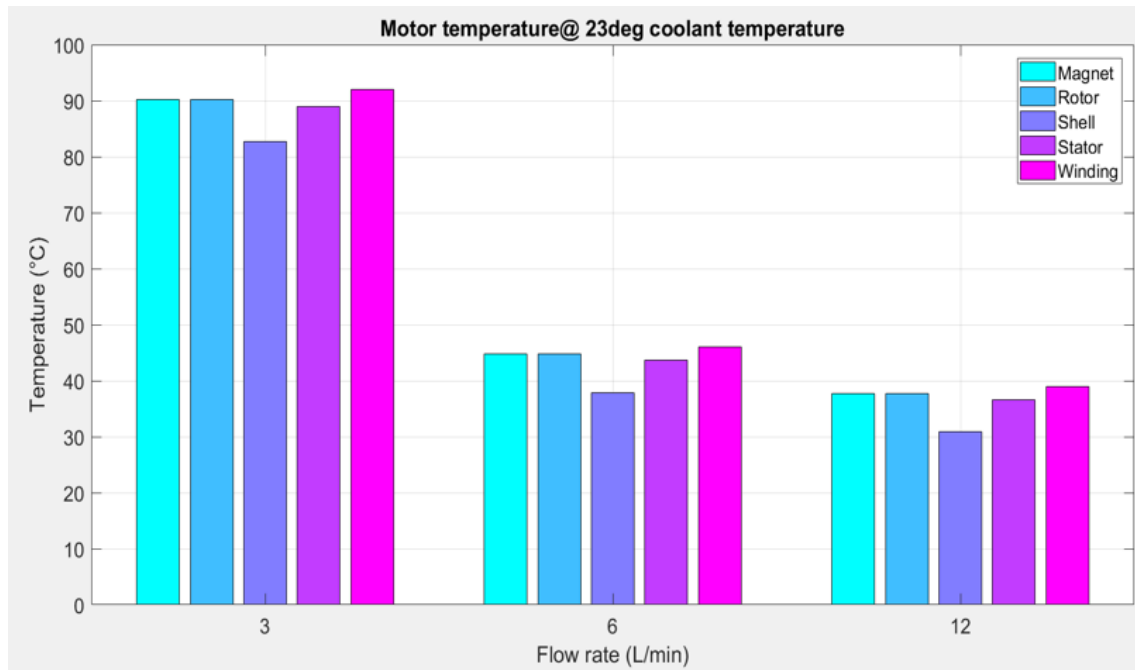


**Figure 4.3:** Temperature distribution of EM parts @ 23deg coolant temperature

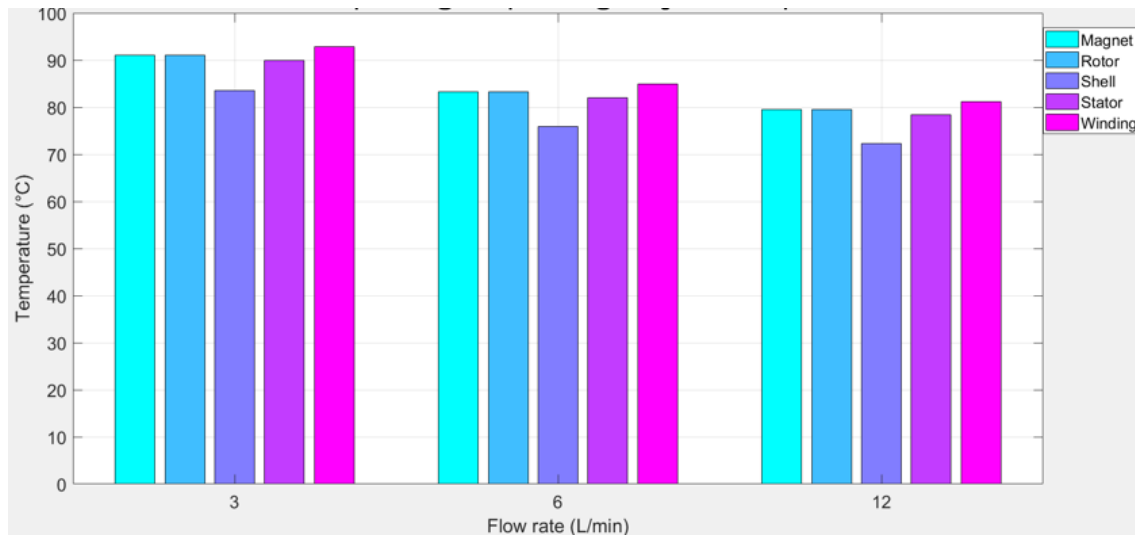
At 23 deg coolant temperatures, the temperature difference between 3 l/min flow rate and 6 l/min was higher than the difference between 6 l/min and 12 l/min. This could be because of the high difference in copper losses and due to low flow rate thus leading to the big difference in temperature. There was a small difference in temperature when the pump is pumping 6 l/min and 12 l/min.

**Table 4.6:** Temperature distribution of EM parts @ 23deg coolant temperature and different flow rates

Flow rate <i>l/min</i>	Magnet <i>deg</i>	Rotor <i>deg</i>	Shell <i>deg</i>	Stator <i>deg</i>	Winding <i>deg</i>
3	90.19	90.19	82.71	89.03	91.95
6	44.76	44.76	37.87	43.63	46.08
12	37.69	37.69	30.90	36.57	38.95

#### 4.2.3.2 Temperature distribution of EM parts @ 65deg coolant temperature

At 65deg coolant temperature the electric machine heated up as shown in Figure 4.4 and Table 4.7.

**Figure 4.4:** Temperature distribution of EM parts @ 65deg coolant temperature**Table 4.7:** Electric machine temperature distribution @ 65deg coolant temperature

Flow rate <i>l/min</i>	Magnet <i>deg</i>	Rotor <i>deg</i>	Shell <i>deg</i>	Stator <i>deg</i>	Winding <i>deg</i>
3	91.09	91.09	83.60	89.92	92.86
6	83.24	83.24	75.86	82.08	84.94
12	79.57	79.57	72.24	78.42	81.23

At 65 deg coolant temperatures, there was a small change in temperatures due to change in flow rate. The highest motor temperatures are observed at 3 l/min.

Temperature distribution of EM parts @ -10 deg coolant temperature At -10 deg coolant temperatures, the electric machine heated up as shown in Figure 4.5 and Table 4.8.

## 4. Results and Analysis

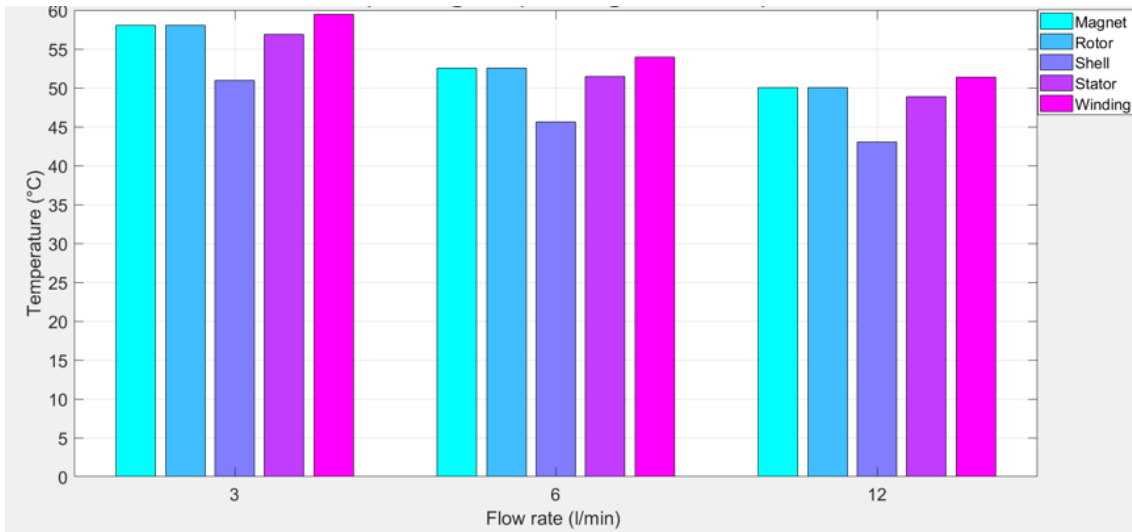


**Figure 4.5:** Electric machine temperature distribution at -10deg coolant temperature

**Table 4.8:** Winding temperatures base verification at -10deg coolant temperature

Flow rate <i>l/min</i>	Magnet <i>deg</i>	Rotor <i>deg</i>	Shell <i>deg</i>	Stator <i>deg</i>	Winding <i>deg</i>
3	58.02	58.02	50.96	56.88	59.47
6	52.58	52.58	45.59	51.44	53.97
12	50.01	50.01	43.06	48.88	51.38

From Table 4.4 it can be seen that at 6 l/min flow rate, the copper losses are higher at -10deg than at 23deg. It was also observed that the temperatures of the machine parts at same flow rate was lower at -10deg than 23deg despite losses being higher. This could be because of the natural cooling of the surrounding.

### 4.3 Steady state analysis at 8000rpm 50Nm

A steady state case set up with 8000rpm and 50Nm was done and the simulated copper and iron losses were as for Figure 4.6 and Table 4.9.

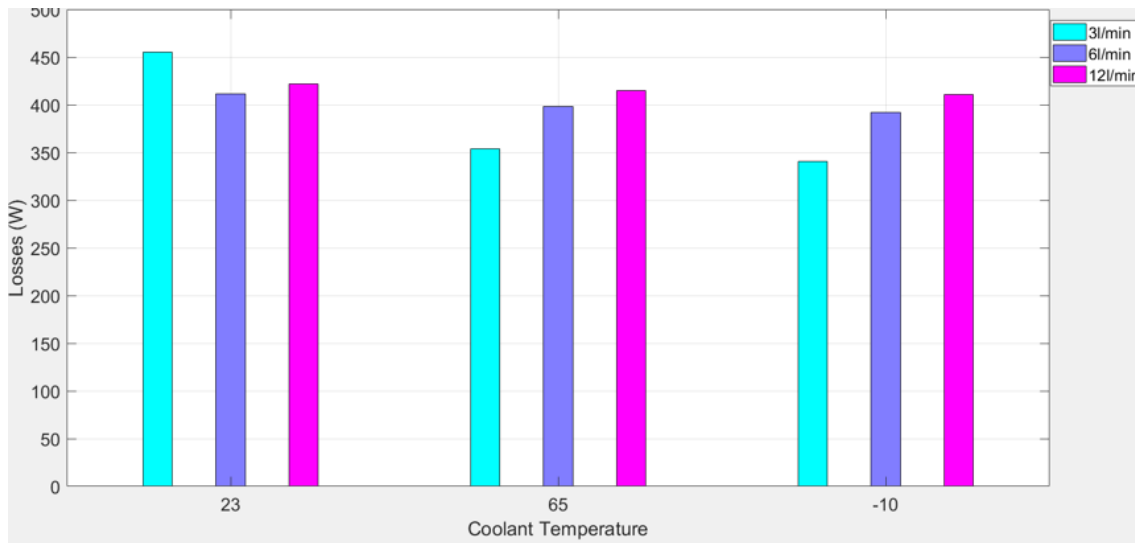


**Figure 4.6:** Simulated losses at 8000rpm 50Nm

**Table 4.9:** Simulated losses at 8000rpm 50Nm.

Flow rate <i>l/min</i>	Pcu <i>W</i> 23	Pcu <i>W</i> 65	Pcu <i>W</i> -10
3	455.17	411.72	421.79
6	354.09	398.33	414.86
12	340.93	391.90	410.90

At this high speed, the copper losses are small compared to the iron losses. They however increase with decrease in flow rate. Iron losses were 2392 watts and remained constant at this specific speed and torque in all coolant temperatures.

### 4.3.1 Electric machine parts temperature distribution at 8000rpm 50Nm

The machine was operated at 8000rpm 50Nm and its' temperature distribution was observed.

#### 4.3.1.1 Temperature distribution of EM parts @ 23 deg coolant temperature

The electric machine parts were investigated at this high speed and the temperature distribution was as shown in Figure 4.7 and Table 4.10.

## 4. Results and Analysis

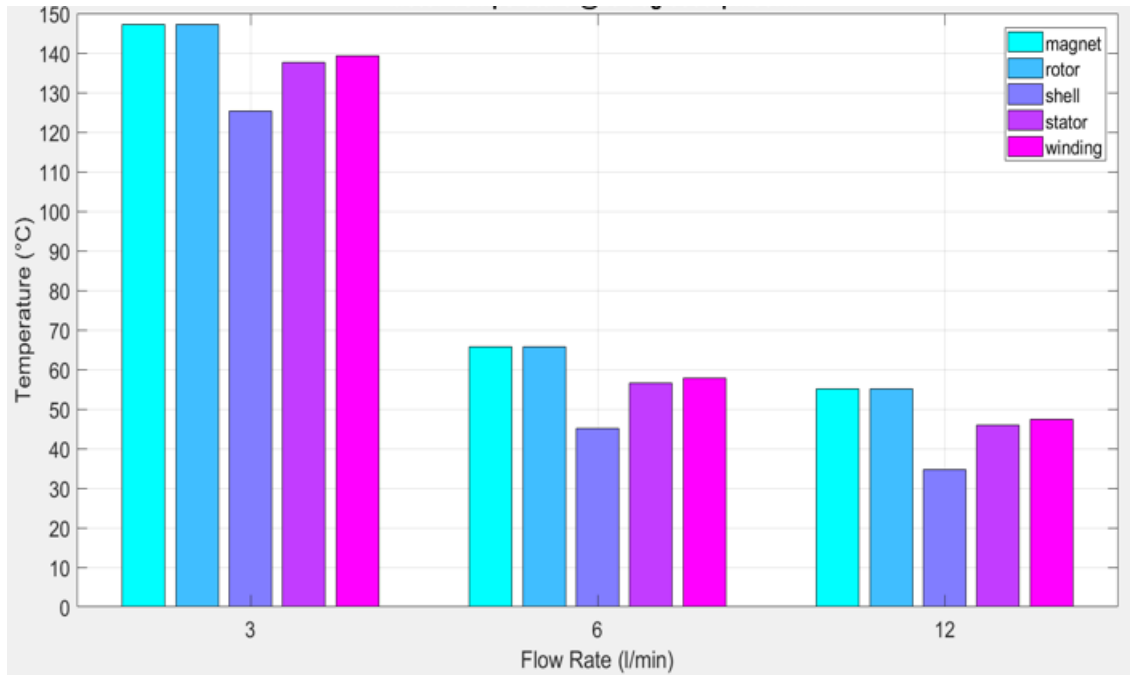


**Figure 4.7:** Machine parts temperature distribution at 23deg 8000rpm 50Nm

**Table 4.10:** Machine part temperature distribution at 23deg 8000rpm 50Nm

Flow rate <i>l/min</i>	Magnet <i>deg</i>	Rotor <i>deg</i>	Shell <i>deg</i>	Stator <i>deg</i>	Winding <i>deg</i>
3	147.27	147.27	125.36	137.54	139.37
6	65.75	65.75	45.20	56.54	57.91
12	55.14	55.14	34.75	45.99	47.30

At flow rate 3 l/min the machine motor parts tend to heat up to high temperatures. It could be that at high speed there is lot of heat generated by the machine and 3 l/min flow rate is not sufficiently cooling thus high temperatures.

### 4.3.1.2 Temperature distribution of the EM parts @ 65 deg

The machine was operated at 8000rpm 50Nm with a coolant temperature of 65 deg and recorded as shown in Figure 4.8 and Table 4.11.

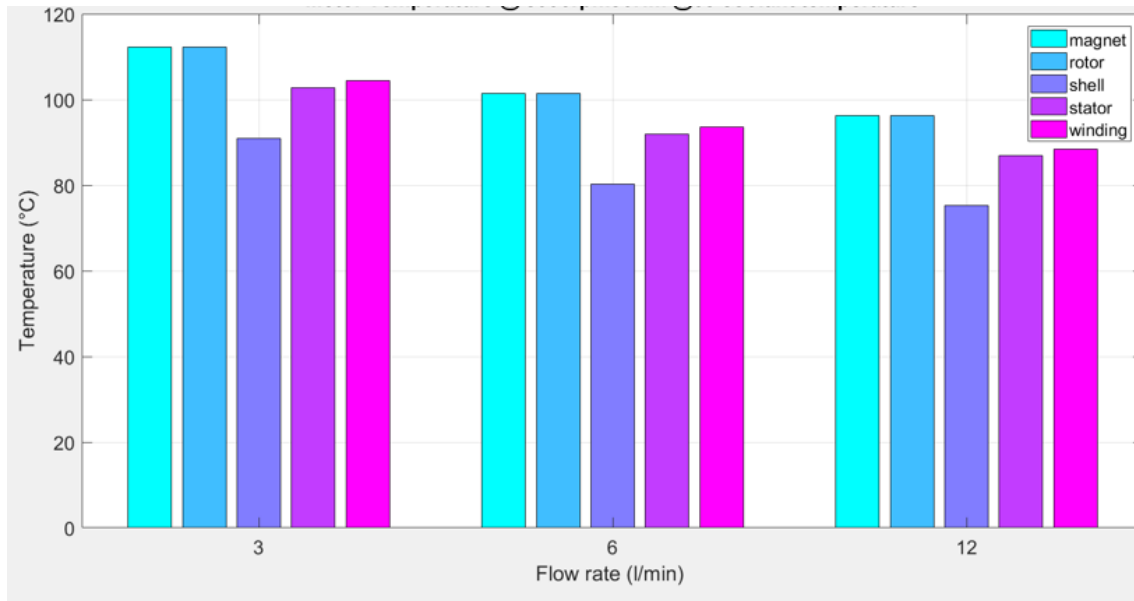


**Figure 4.8:** Machine part temperature distribution at 65deg 8000rpm 50Nm

**Table 4.11:** Electric machine parts temperature distribution at 65deg 8000rpm 50Nm

Flow rate <i>l/min</i>	Magnet <i>deg</i>	Rotor <i>deg</i>	Shell <i>deg</i>	Stator <i>deg</i>	Winding <i>deg</i>
3	112.23	112.23	90.92	102.73	104.36
6	101.43	101.43	80.31	92.00	93.57
12	96.24	96.24	75.20	86.84	88.38

#### 4.3.1.3 Electric machine parts temperature distribution at -10deg

Temperature distribution of the electric machine parts at -10 deg was as shown in Figure 4.9 and Table 4.12.

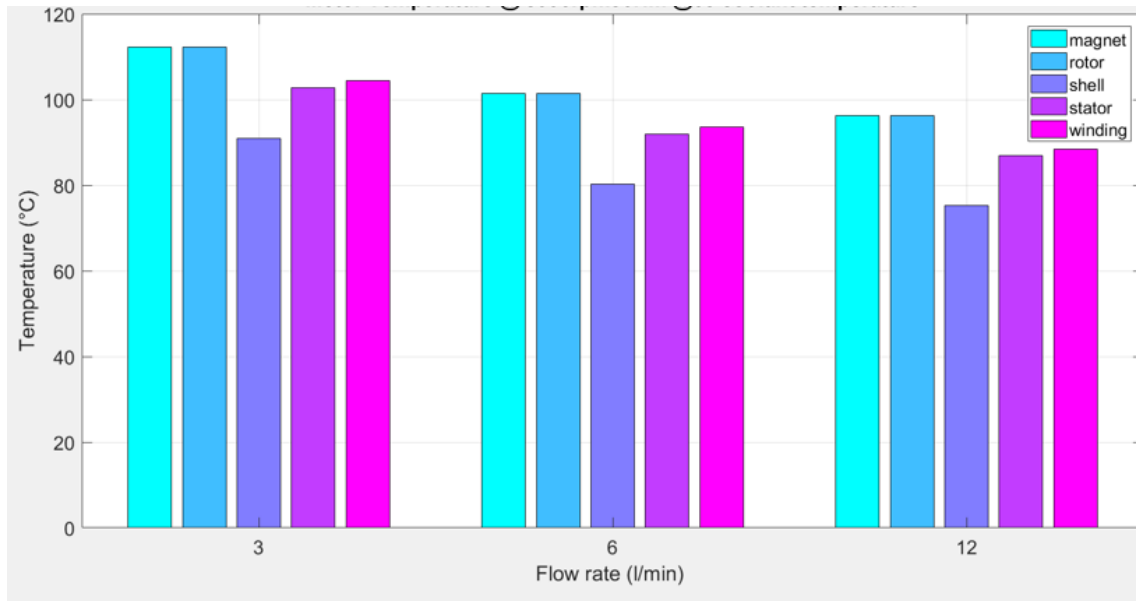


**Figure 4.9:** Temperature distribution on EM parts at -10deg 8000rpm 50Nm

**Table 4.12:** Temperature distribution on EM parts at -10deg 8000rpm 50NM

Flow rate <i>l/min</i>	Magnet <i>deg</i>	Rotor <i>deg</i>	Shell <i>deg</i>	Stator <i>deg</i>	Winding <i>deg</i>
3	120.34	120.34	98.91	10.79	112.47
6	114.76	114.76	93.41	105.24	106.89
12	111.56	111.56	90.27	102.07	103.69

At this high speed level -10 and 65 degrees coolant temperatures have high temperatures in all the flow rates. The motor doesn't cool much despite increase in flow rate.

In -10 degrees, it could be that the coolant becomes thick and heavy thus can not be pumped efficiently.

### 4.3.2 Comparison between losses at high speeds and low speeds

A comparison was made between copper losses at 8000rpm 50Nm and 4000rpm 100Nm as shown in Figures 4.10 and 4.11.

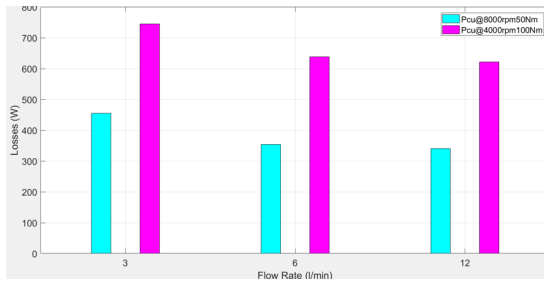


**Figure 4.10:** Copper losses at 4000rpm 100Nm and 8000rpm 50Nm

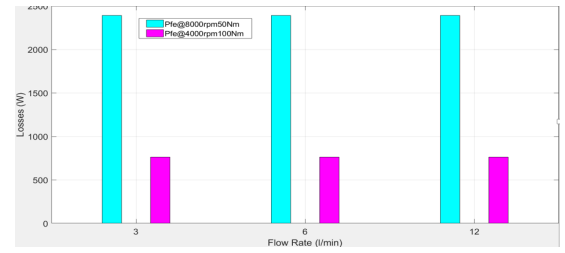


**Figure 4.11:** Iron losses at 4000rpm 100Nm and 8000rpm 50Nm

At low speed the copper losses dominate but at high speeds the iron losses dominate.

### 4.3.3 Simulated, measured and manufacturers' copper losses

The three copper losses were compared as shown in Figure 4.12. There was a slight difference between measured data and simulated data. This could be caused by the measuring instrument errors.

There was a difference between measured and manufacturers' copper losses. This could be because of the period of time the manufacturer operated the machine is unknown. It could also be because the flow rate the manufacturer is using to cool the machine is also unknown.

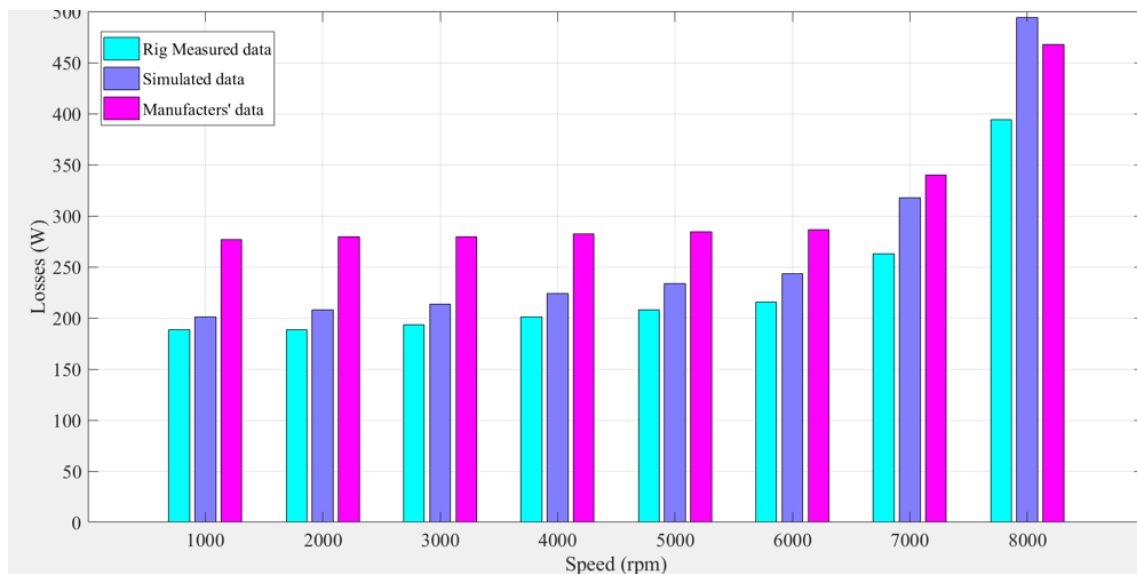


**Figure 4.12:** Simulated, measured and manufacturers' copper losses at 50Nm

## 4. Results and Analysis

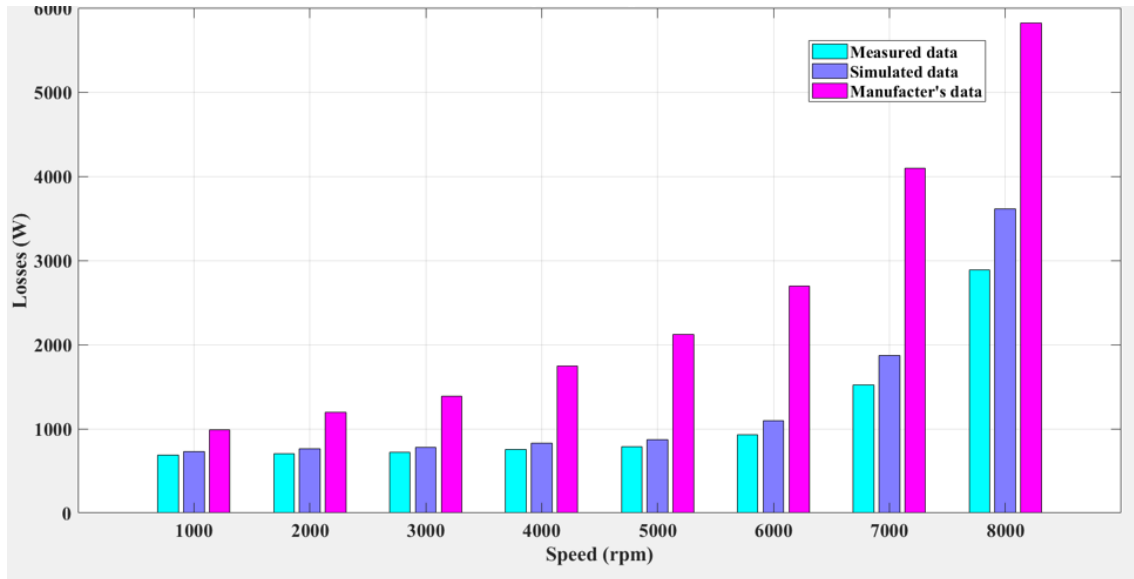


**Figure 4.13:** Simulated, Measured and manufacturers' copper losses at 4000rpm 100Nm

### 4.4 Pump power consumption

At 4000rpm 100Nm pump power consumption in watts was investigated at different flow rate and coolant temperatures. The pump power consumption was also done at 8000rpm 50Nm and the difference in power consumption was small. The results shown in Figure 4.14 and table 4.13 are for 4000rpm 100Nm.

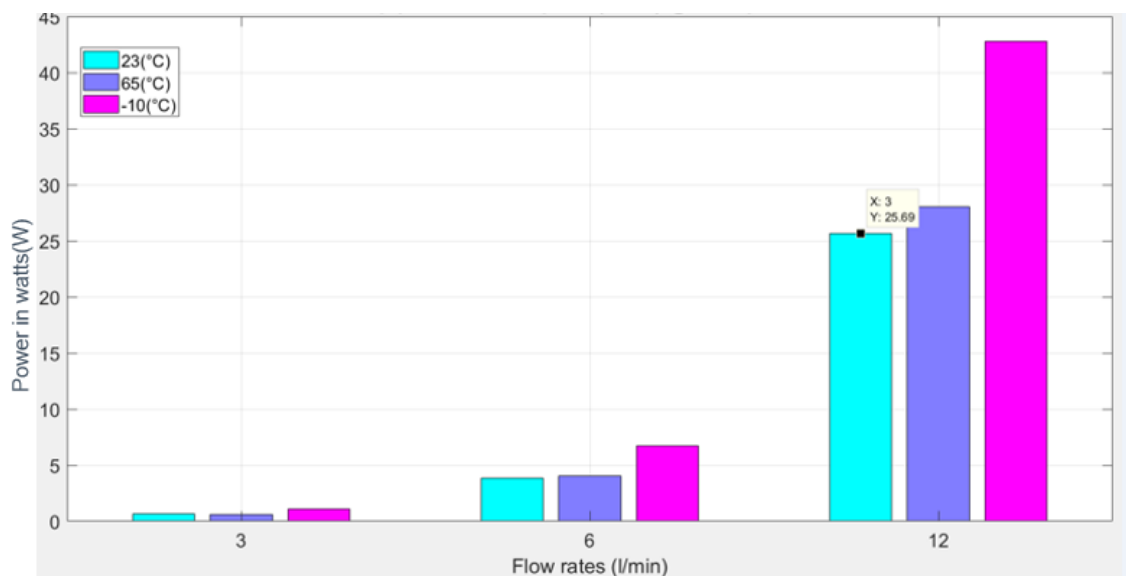


**Figure 4.14:** Pump power consumption at different flow rates

The coolant pump consumed little energy to pump 3 l/min flow rate in all coolant temperatures. Although at same flow rate, the pump used more energy at -10 degree

**Table 4.13:** Pump power consumption at 4000rpm 100Nm and different flow rates

<b>Flow rate</b> <i>l/min</i>	<b>23</b> <i>deg</i>	<b>65</b> <i>deg</i>	<b>-10</b> <i>deg</i>
3	0.640	0.588	1.078
6	3.839	4.028	6.719
12	25.686	28.025	42.776

coolant temperature. As the flow rate increased, so did the power consumed. There was a spike in power consumption to pump 12 l/min compared to 6 l/min in all coolant temperatures. The pump consumed most power to pump 12 l/min during the -10 degree coolant temperatures. This could be because of the different fluid dynamics and properties during such low temperatures.

The coolant becomes thick and heavier thus the pump used more power to pump 12 l/min. From previous, it was observed that there was no big difference in motor temperatures whether the pump pumps 12 l/min or 6 l/min.

## 4.5 Drive Cycle Operation

In the WLTC drive cycle, at 6 l/min and 23, 65 and -10 degrees coolant temperatures, the copper losses are high during high speed driving. They are observed highest at 65 degrees coolant temperature as shown in Figure 4.20 and 4.21.

## 4. Results and Analysis

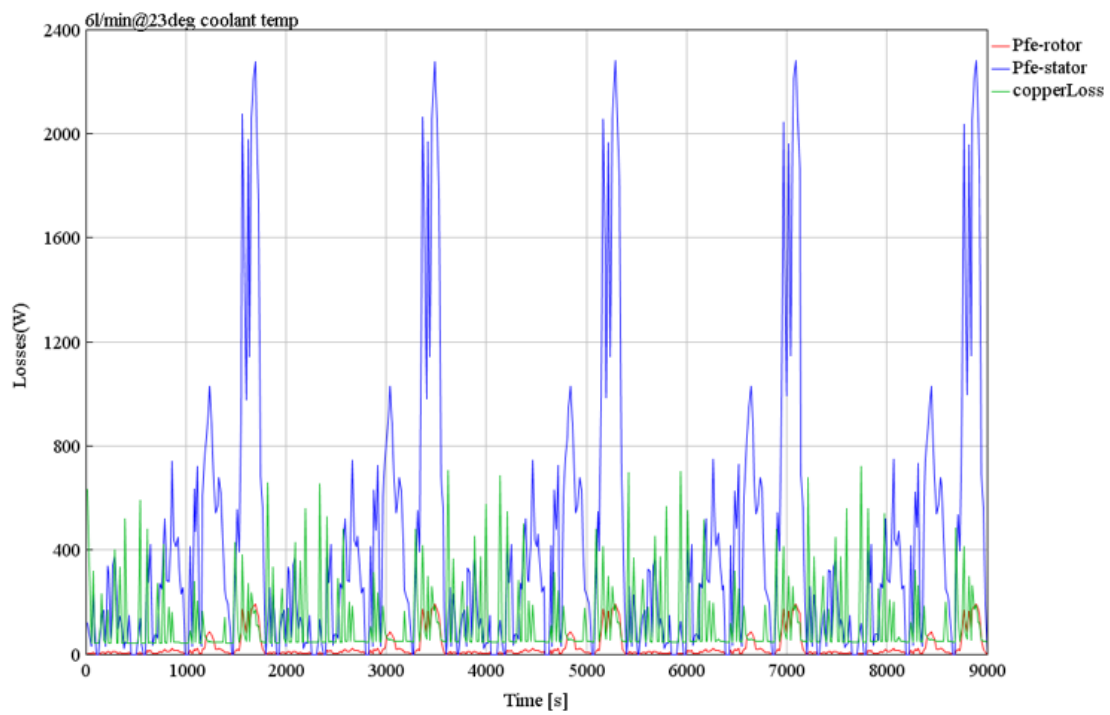


Figure 4.15: figure

Losses on WLTC drive cycle

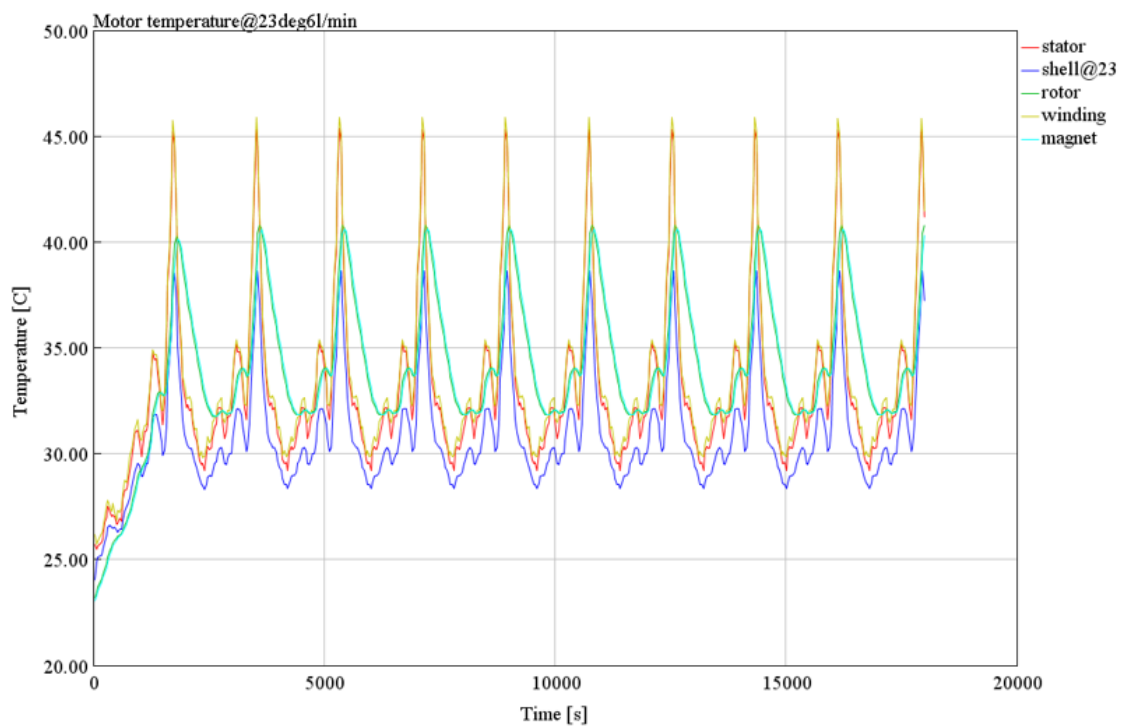


Figure 4.16: figure

Machine temperature distribution on WLTC drive cycle

Iron losses dominate at the end of the drive cycle where the speed is high. The winding have the highest temperature at the end of the drive cycle.

## 4.6 Radiator dimension variation

Losses were investigated for different sizes of the radiator at a fixed flow rate to find optimal size for this specific loop and was as shown in figure 4.15.

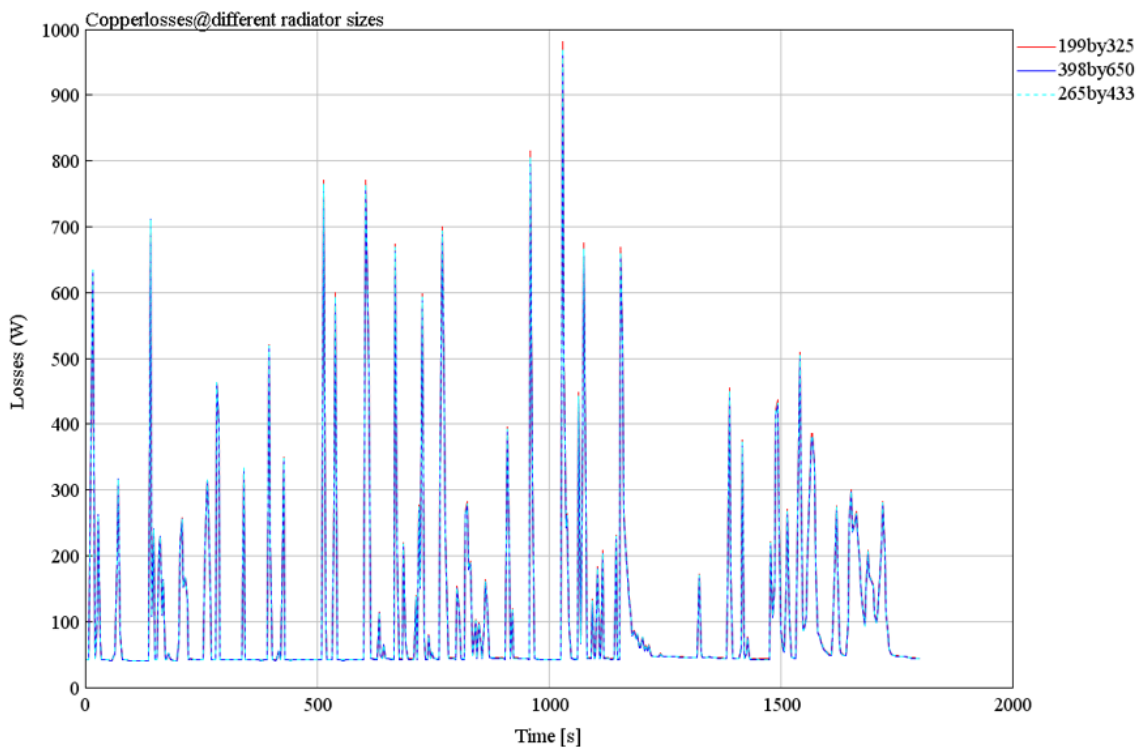


**Figure 4.17:** Copper losses of the radiator at different sizes

There was a slight difference in losses between the radiator sizes. The highest copper losses were experienced when the radiator was reduced by 50 percent. This means that if the radiator could be halved, there would be little change in losses but significant change in energy efficiency.

Figure 4.16 shows the heat transfer of the radiator at different sizes.

#### 4. Results and Analysis

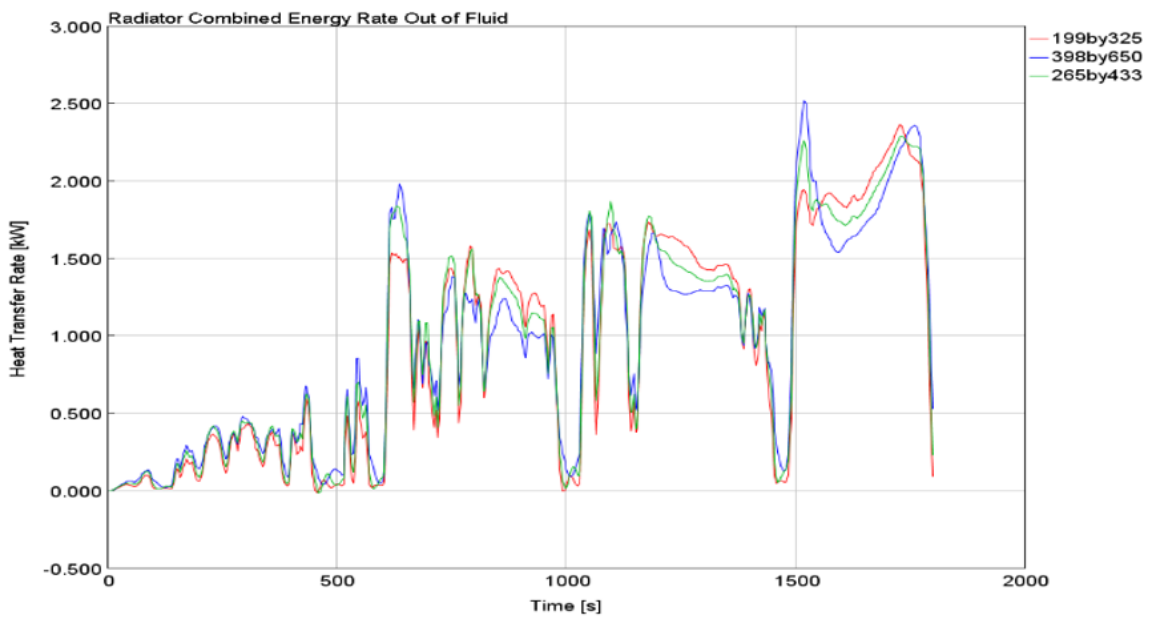


**Figure 4.18:** Heat transfer of the radiator at different sizes

From the figure it shows that heat was transferred least when the radiator was reduced by 50 percent but the difference was small between full size and halved. Since the windings are the most important heat source the effect of different radiator sizes was done and the temperature distribution was as in Figure 4.17.

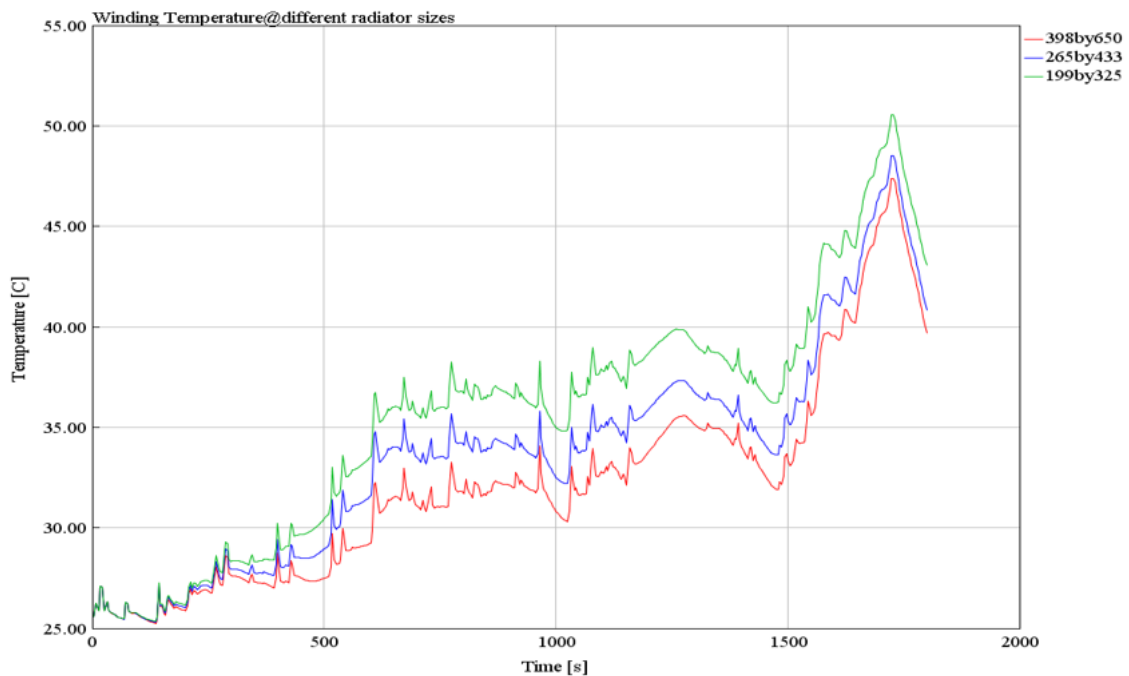


**Figure 4.19:** Winding temperature at different radiator sizes

When the radiator is reduced by 50 percent and at time 1000 secs, the winding heat up 32deg and when at full length the winding heat up at 35 deg. This is a small difference in cooling so this radiator can be reduced in size.

## 4.7 Fan signal point variation

From the design of this fan, it switches on at point zero when the coolant temperature is at 60 deg and at full speed when at point 1 when the coolant temperature is at 65 deg. An interpolation was done between 0 and 1. An investigation of the interpolated signals was done so as to find a suitable operating point of the fan. Its' power consumption was also investigated at these signals .The results were as shown in Figure 4.18 and Table 4.14.

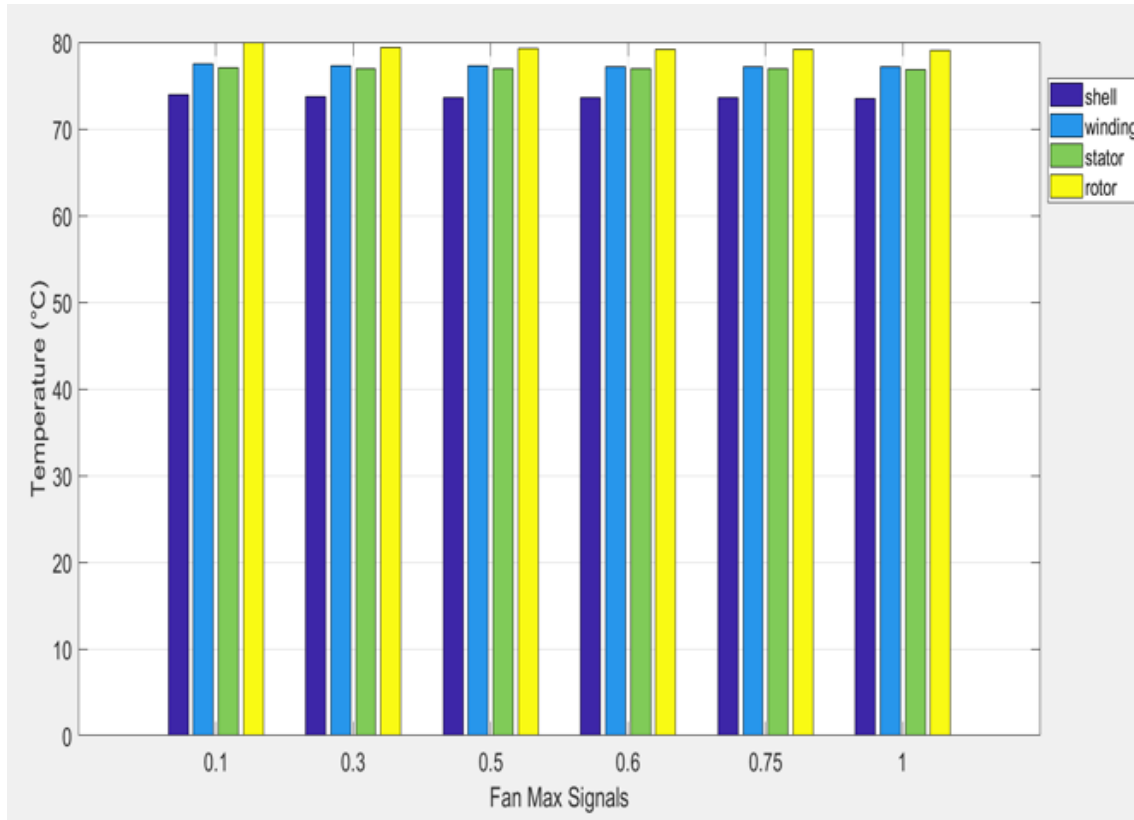


**Figure 4.20:** Fan operating at different signals

**Table 4.14:** Temperature distribution on EM at different fan signals

Fan signals	shell	winding	stator	rotor
–	<i>deg</i>	<i>deg</i>	<i>deg</i>	<i>deg</i>
0.1	73.90	77.50	77.10	79.91
0.3	73.70	77.30	76.96	79.40
0.5	73.60	77.23	76.90	79.30
0.6	73.60	77.20	76.89	79.20
0.75	73.60	77.18	76.90	79.15
1	73.50	77.12	76.80	79.10

There is a slight change in temperatures in the machine parts when the fan signals change from signal 0.1 to 1. The fan is perhaps over dimesioned. The fan consumed

## 4. Results and Analysis

---

power as shown in Figure 4.19 and Table 4.15 during this operating signals.

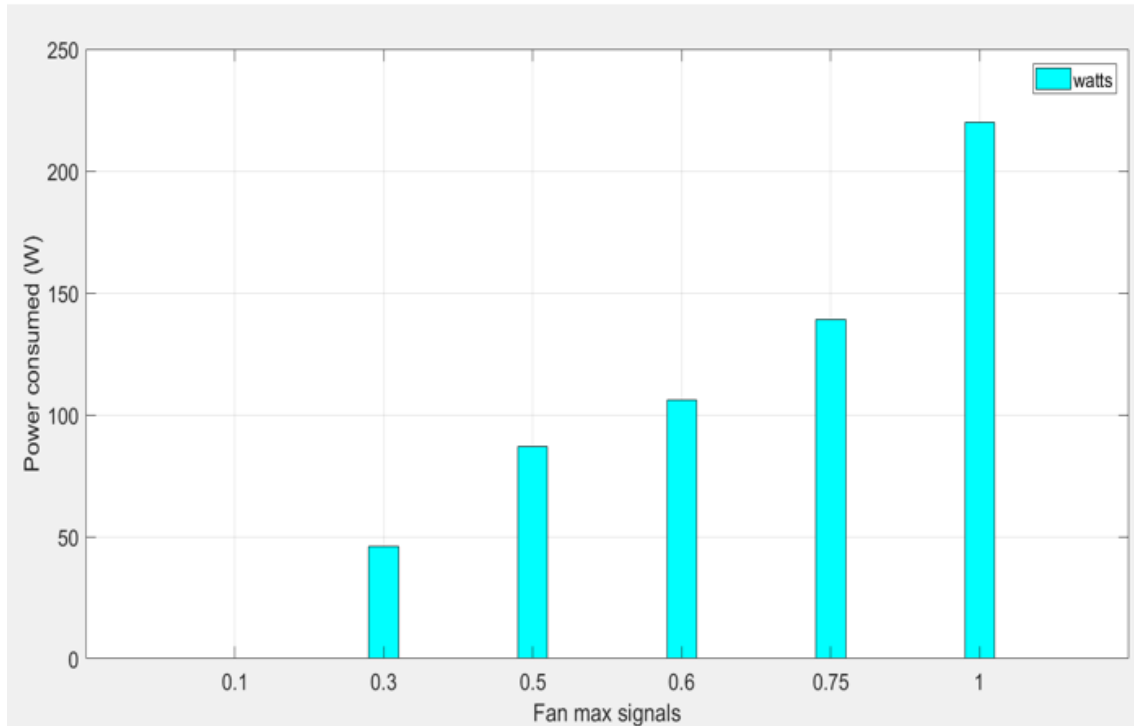


**Figure 4.21:** Fan power consumption at different signals

**Table 4.15:** Fan operating signals

Fan max signals	Power	speed
—	<i>watts</i>	<i>rpm</i>
0.1	0	0
0.3	46	1208
0.5	87	1582
0.6	106.2	1710
0.75	138.8	1902
1.0	220	2253

The fan consumes power as shown above but cooled the machines' parts slightly. There is a room to operate at different signal and save energy on the loop.

# 5

## Conclusion

A model of propulsion cooling loop has been implemented in GT-suite and investigated. Motor internal temperatures are highly influenced by the coolant temperatures and the flow rate. Pump power consumption increases with increase in flow rate. Radiator size reduction in this particular study would save cost of production and maintain almost the same cooling.

At high speeds the iron losses dominate the copper losses at steady state and drive cycle. In this particular study the fan could operate at a lower signal than 1 and save the entire loop energy.

### 5.1 Future work

An optimization for this entire loop could be done in the future. Motor design could be improved by bringing the coolant closer to the windings which are the greatest source of heat for example with a hair pin motor design and rectangular cooling tubes



# Bibliography

- [1] Mohan, Undeland and Robins: Power Electronic, Converters, Application and Design.
- [2] Emma Arfa Grunditz Design and Assessment of Battery Electric Vehicle Power Train, with Respect to Performance, Energy Consumption and Electric Motor Thermal Capability.
- [3] A. Wintrich, U. Nicolai, W. Tursky, and T. Reimann. (2011) Application manual power semiconductors. Semikron International GmbH. [Online]. Available:[http://www.semikron.com/skcompub/en/SEMIKRON Application Manual Power Semiconductor.pdf](http://www.semikron.com/skcompub/en/SEMIKRON_Application_Manual_Power_Semiconductor.pdf)
- [4] J.P Holman, Heat Transfer, McGraw-Hill, London, 1992
- [5] Y.K. Chin, D.A. Staton, “ Transient Thermal Analysis using both Lumped-Circuit Approach and Finite Element Method of a Permanent Magnet Traction Motor”
- [6] Demetriades, H. De La Parra, E. Andersson, and H. Olsson, “A real-time thermal model of a permanent-magnet synchronous motor,” Power Electronics, IEEE Transactions on, vol. 25, no. 2, pp. 463–474, Feb 2010.
- [7] Y. A. Çengel, Introduction to Thermodynamics and Heat Transfer. McGraw-Hill, 2008
- [8] A. F. Mills, Heat Transfer. Prentice-Hall Inc., 1999.
- [9] D. Staton, S. PICKERING, and D. LAMPARD, “Recent advancement in the thermal design of electric motors,” in SMMA 2001 Fall Technical Conference "Emerging Technologies for the Electric Motion Industry", Raleigh-Durham, North Carolina, USA, Oct 2001.
- [10] F. Incropera, D. Dewitt, T. Bergman, and A. Lavine, Fundamentals of Heat and Mass Transfer. John Wiley Sons, 2007
- [11] G. Kylander, “Thermal modelling of small cage induction motors,” Thesis for the degree of Doctor of Philosophy in Engineering, Technical Report No. 265 Chalmers University of Technology, Feb 1995.
- [12] Parsippany NJ, Introduction to centrifugal pumps Fundamentals:[Online] Available:<https://www.intropumps.com/pumps-101/what-is-a-centrifugal-pump/>
- [13] Available:[Online]:<http://www.brushless-dcmotor.com/sale-10304794-aluminum-alloy-auto-electric-water-pump-12-volt-electric-coolant-pump-for-hybrid-electrical-vehicle.html> Accessed July 2018

## Bibliography

---

- [14] Available:[Online]:<https://www.speedwaymotors.com/AFCO-1949-54-Chevy-Aluminum-Radiator-Chevy-Engine,53646.html> Accessed July 2018
- [15] Available:[Online]:<https://www.onallcylinders.com/2012/07/24/mechanical-vs-electric-fans-which-best-your-vehicle/> Accessed July 2018
- [16] Available:[Online]:<https://askchina.me/q/-24423446772> Accessed July 2018
- [17] Available:[Online]:<https://www.nikkan.co.jp/articles/view/00432369> Accessed July 2018
- [18] Available:[Online]:<https://wiki.anton-paar.com/en/automotive-antifreeze/> Accessed July 2018